Contrib Mineral Petrol (2011) 162:797–819
DOI 10.1007/s00410-011-0625-4

ORIGINAL PAPER

Fluid/rock interaction and mass transfer in continental subduction zones: constraints from trace elements and isotopes (Li, B, O, Sr, Nd, Pb) in UHP rocks from the Chinese Continental Scientific Drilling Program, Sulu, East China

Yilin Xiao · Jochen Hoefs · Zhenhui Hou · Klaus Simon · Zeming Zhang

Received: 23 September 2010 / Accepted: 7 March 2011 / Published online: 19 April 2011

Abstract In order to better understand the role of fluids during subduction and subsequent exhumation, we have investigated whole-rock and mineral chemistry (major and trace elements) and Li, B as well as O, Sr, Nd, Pb isotopes on selected continuous drill-core profiles through contrasting lithological boundaries from the Chinese Continental Scientific Drilling Program (CCSD) in Sulu, China. Four carefully selected sample sets have been chosen to investigate geochemical changes as a result of fluid mobilization during dehydration, peak metamorphism, and exhumation of deeply subducted continental crust. Our data reveal that while O and Sr-Nd-Pb isotopic compositions remain more or less unchanged, significant Li and/or B isotope fractionations occur between different lithologies that are in close contact during various metamorphic stages. Samples that are supposed to represent prograde dehydration as indicated by veins formed at high pressures (HP) are characterized by element patterns of highly fluid-mobile elements in the veins that are complementary to those of the host eclogite. A second sample set represents a UHP metamorphic crustal eclogite that is separated from a garnet peridotite by a thin transitional interface. Garnet peridotite and eclogite are characterized by a >10% difference in MgO, which, together with the presence of abundant hydroxyl-bearing minerals and compositionally different clinopyroxene grains demonstrate that both rocks have been derived from different sources that have been tectonically juxtaposed during subduction, and that hydrous silicate-rich fluids have been added from the subducting slab to the mantle. Two additional sample sets, comprising retrograde amphibolite and relatively fresh eclogite, demonstrate that besides external fluids, internal fluids can be responsible for the formation of amphibolite. Li and B concentrations and isotopic compositions point to losses and isotopic fractionation during progressive dehydration. On the other hand, fluids with isotopically heavier Li and B are added during retrogression. On a small scale, mantle-derived rocks may be significantly metasomatized by fluids derived from the subducted slab. Our study indicates that during high-grade metamorphism, Li and B may show different patterns of enrichment and of isotopic fractionation.

Keywords Fluid/rock interaction · Elemental transfer · Isotopic fractionation · Subduction and exhumation · Sulu

Communicated by T. L. Grove.

Electronic supplementary material The online version of this article (doi:10.1007/s00410-011-0625-4) contains supplementary material, which is available to authorized users.

Y. Xiao (✉) · Z. Hou
CAS Key Laboratory of Crust-Mantle Materials and Environments, School of Earth and Space Sciences, University of Science and Technology of China, 230026 Hefei, China
e-mail: ylxiao@ustc.edu.cn

Y. Xiao · J. Hoefs · K. Simon
Geowissenschaftliches Zentrum der Universität Göttingen, Goldschmidtstrasse 1, 37077 Göttingen, Germany

Z. Zhang
Institute of Geology, Chinese Academy of Geological Sciences, 100037 Beijing, China

Introduction

It is well known that subduction of altered basaltic oceanic crust and overlying sediments is characterized by significant releases of aqueous fluids from metamorphosing slabs (Bebout 2007; Forneris and Holloway 2003; Jarrard 2003;

Peacock 1990). Since subducted oceanic material rarely returns back to the surface, inferences about the fluid inventory during subduction relies on indirect evidence, such as the analysis of arc rocks. In contrast, deeply subducted continental crust is usually brought back to the surface due to its lower density. However, only limited attention has been paid so far to the role of fluids during subduction and exhumation of continental crust (e.g., Zheng 2009). In comparison with hydrated oceanic crust, subducted continental crust is drier, commonly older and colder, less dense, and enriched in incompatible elements. Nevertheless, subducted continental materials must have been subjected to dehydration, releasing fluids from the subducting slab. Substantial amounts of H_2O may have been transported to depths of more than 100–200 km by hydrous minerals during UHP metamorphism (Poli and Schmidt 1995; Thompson 1992). Volatiles released by decomposition of hydrous phases may enter the structure of anhydrous mantle minerals (Su et al. 2004; Xia et al. 2005).

Lithium (Li), boron (B) and oxygen (O) isotopes are excellent tracers for fluid/rock interactions during downgoing and uplift processes of subducted slabs (e. g., Elliott et al. 2006; Ionov and Seitz 2009; Leeman et al. 2004; Magna et al. 2006; Moriguti and Nakamura 1998; Moriguti et al. 2004; Teng et al. 2007; Tomascak 2004). Early Li and B isotope analyses have highlighted the behavior of these elements under hydrothermal and low-temperature conditions, with the heavier isotopes (^{7}Li and ^{11}B) becoming enriched in fluid phases (Chan et al. 1992; Hervig et al. 2002; Hoefs and Sywall 1997; Palmer and Swihart 1996; Rudnick et al. 2004; Seyfried et al. 1998). Recently, experimental work documented the partitioning and isotopic fractionation of Li and B between fluids and minerals at higher temperatures (e.g., Wunder et al. 2005, 2006; Meyer et al. 2008). Interestingly, at high temperatures, B isotopes vary regularly with the degree of B enrichment, whereas Li isotopes do not correlate in such a general way (e.g., Elliott et al. 2004; Tomascak et al. 2002). Although extremely low δ^{7}Li values in HP eclogites have been reported, the cause for the depletion of Li isotopes is unclear (Agostini et al. 2008; Marschall et al. 2007a; Simons et al. 2010; Zack et al. 2003). Thus, apparently isotopes of the two elements may behave differently at high-temperature conditions. At mantle conditions, Li can be incorporated into magnesian silicates while B is dominantly fluid controlled (Bebout et al. 1993; Seyfried et al. 1998). Consequently, the Li and B systematics may provide a record of fluid/rock and crust/mantle interactions in deep subduction zones.

The Dabie–Sulu UHP metamorphic belt, which is the largest known UHP terrain, is a suitable region to study the fluid regime of subducted crustal material, because of its abundant veins that formed during subduction (Castelli et al. 1998; Franz et al. 2001) and exhumation (Wu et al. 2009; Zheng et al. 2007). Furthermore, variable extents of fluid/melt metasomatism are evident at contacts between different lithological units (Zhao et al. 2007). In this paper, we outline the petrology, bulk-rock and mineral geochemistry, and isotope systematics of four carefully selected sample sets collected from drill cores of the Chinese Continental Scientific Drilling program (CCSD), representing different stages of fluid/rock interaction. We investigate elemental and isotopic fractionations, during (i) prograde metamorphism, (ii) peak metamorphic conditions, and (iii) retrograde exhumation. Of special relevance in our study are investigations into Li and B concentrations and isotopic compositions.

Geological background and samples

The CCSD has been carried out in the Dabie–Sulu metamorphic belt at Donghai with a final depth of 5,158 m for the main hole (Xu 2007). Orthogneiss, paragneiss, eclogite, amphibolite (mostly retrograded from eclogite), and ultramafic rocks are the main rock types that have been drilled; rarely, schist, and quartzite occur as thin interlayers within paragneiss and eclogite (for details, see Zhang et al. 2006). The overall thickness of eclogites is about 1,200 m. A garnet peridotite sequence, which is sandwiched by normal or quartz-rich eclogite at the base and highly Fe–Ti-enriched eclogite at the top, has been recovered from 603.2 to 683.5 m (Yang et al. 2007). High-pressure veins with eclogite-facies mineral assemblages and retrograde veins with amphibolite-facies mineral assemblages are commonly observed in the eclogite cores (e.g., Xu 2007; Zhang et al. 2008). All rock types down to 5,158 m from the CCSD have been subjected to UHP metamorphism, as documented by the preservation of coesite inclusions in zircon (Liu et al. 2007).

Samples for this study were collected from small-scale CCSD continuous profiles (Fig. 1). After general inspection of the drill cores, we carefully selected four sets of samples that in our view are rocks formed during different metamorphic stages, ranging from (i) prograde dehydration through (ii) metamorphic peak conditions to (iii) retrogression during exhumation. Sample sets of 1, 3, and 4 were collected from 312.7 (CCSD-1-Ec and CCSD-1-Hv), 369.1 (CCSD-3-Ec and CCSD-3-Am), and 511.0 m (CCSD-4-Ec and CCSD-4-Am) of the CCSD main hole, whereas sample set 2 (CCSD-2-Gp, CCSD-2-Tr, and CCSD-2-Ec) was from drill-hole ZK703, which is about 80 m away from the main hole (Xiao et al. 2006). Sample set 1 (Fig. 1a) contains hydrous veins and consists of high-pressure mineral assemblages like phengite, quartz, and clinopyroxene formed during prograde dehydration of eclogites that are regarded to represent direct samples formed during

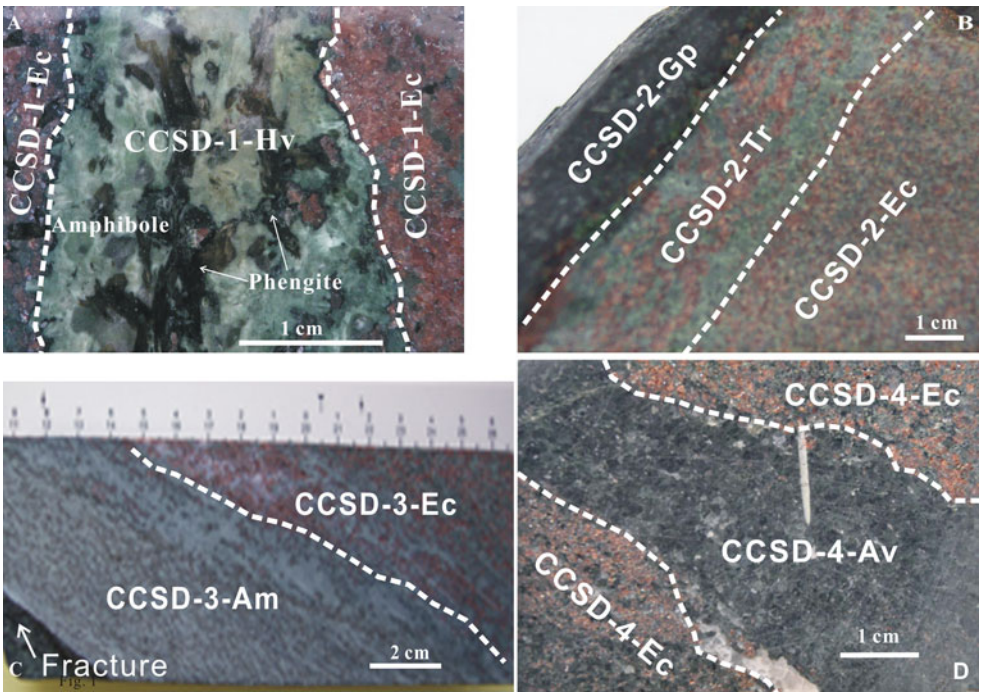

Fig. 1 Investigated samples showing small-scale distinguishable lithologies collected from drill cores of the Chinese Continental Scientific Drilling Program. **a** Shows a HP vein in the center (*CCSD-1-Hv*) and dehydrated eclogite on both sides (*CCSD-1-Ec*); **b** represents the transition from garnet peridotite to eclogite with a transition zone; **c** and **d** comprise retrograde amphibolite and relatively fresh eclogite

subduction dehydration (Becker et al. 1999; Castelli et al. 1998; Spandler and Hermann 2006).

Peridotites enclosed within UHP metamorphic rocks (sample set 2; Fig. 1b) provide an excellent natural laboratory to study fluid-controlled metasomatism in a slab/mantle system (e.g., Marocchi et al. 2007, 2009; Malaspina et al. 2009). Of particular interest are garnet peridotites, as a minimum pressure of 1.6 GPa is required to stabilize garnet under lherzolitic compositions (e.g., Green and Ringwood 1967; O'Neill 1981; Robinson and Wood 1998). Retrograde veins (sample set 3 and 4; Fig. 1c, d) formed during uplift and cooling typically contain amphibole and plagioclase that differ from the phase assemblages in high-pressure veins and thus are suitable to study fluid/rock interaction during exhumation (Barnicoat and Fry 1986).

Mineral assemblages of investigated samples are shown in Table 1. Metamorphic P–T conditions of the sampled eclogites and garnet peridotite were calculated using experimentally and empirically calibrated geothermometers and geobarometers involving equilibria of garnet (Grt), omphacite (Cpx), orthopyroxene (Opx), and phengite. The minimum pressure of peak metamorphism for all investigated eclogites can be assumed to be >2.8 GPa, because of inclusions of quartz pseudomorphs after coesite and because of coesite inclusions in zircons (Liu et al. 2007). The results of P–T calculations are summarized in Table 2.

Sample set 1: dehydrated eclogite (CCSD-1-Ec) and high-pressure vein (CCSD-1-Hv)

This sample set consists of an eclogite and a cm-thick "pegmatite-like" vein (Fig. 1a). The host eclogite (CCSD-1-Ec) contains garnet, omphacite, phengite, and minor quartz and rutile, which may represent a dehydrated relic. Generally, minerals in the eclogite are relatively fresh and free from visible retrogression. However, slight retrogression is evident by the presence of amphibole after omphacites and phengites with low SiO_2 in the rims. The pegmatite-like HP "vein" (CCSD-1-Hv; ~2 cm wide) contains coarse-grained phengite (up to 1 cm in size, Fig. 1a), quartz, omphacite, amphibole (at the rim of omphacite), and rare garnet. The coarse-grained phengite is parallel to the strike direction of the vein. Omphacite occurs both in the matrix and as inclusions in garnet (Fig. 2a). Omphacite in the matrix may be partially replaced and rimmed by late symplectite of clinopyroxene + sodic amphibole + albitic plagioclase. Rutile and apatite are accessory phases.

Using the Grt–Cpx–phengite geobarometer of Carswell et al. (1997) for temperatures of 800°C, pressures of 2.4–2.7 GPa at the rim and of 3.4–3.5 GPa at the core were obtained for phengites from the eclogite and from the vein of 2.6–2.9, 3.4–3.5, and 2.5–2.6 GPa at the rim, the central

Table 1 Mineral assemblages of investigated samples

Sample No.	Lithology	Garnet	Clinopyroxene	Orthopyroxene	Olivine	Amphibole	phengite	Quartz	Albite	Chlorite	Rutile	Ilmenite	Chromite	Pyrite	Zircon
HP vein and host eclogite															
CCSD-1-Hv	High-P vein	x	x	–	–	r	x	x	r	–	x	r	–	–	t
CCSD-1-Ec	host eclogite	x	x	–	–	r	x	x	–	–	x	r	–	–	t
Coexisting garnet peridotite/eclogite															
CCSD-2-Gp	garnet peridotite	x	x	–	x (ss)	–	–	–	–	–	–	exfr	t	–	–
CCSD-2-Tr	transition zone	x	x	t	t (ss)	x	–	–	–	r	?	exfr	–	t	–
CCSD-2-Ec	eclogite	x	x	–	–	tr	–	–	–	–	t	r	–	–	?
Coexisting amphibolite and eclogite															
CCSD-3-Ec	eclogite	x	x	–	–	r	–	x	–	–	x	r	–	–	t
CCSD-3-Am	amphibolite	x	i	–	–	x	–	x	x	x	i	r	–	–	t
CCSD-4-Av	amphibolite	x	i	–	–	x	–	x	x	–	x	r	–	–	t
CCSD-4-Ec	eclogite	x	x	–	–	r	x	x	–	?	x	r	–	–	t

exfr exsolved from; *i* only occurs as inclusion phase; *r* mineral is a minor retrograde phase; *ss* serpentinization; *t* trace amount; *x*, present as major phase; –, not observed

portion, and the core, respectively (Table 2). Temperatures, estimated by applying the garnet–clinopyroxene geothermometers of Ellis and Green (1979); Krogh (1988) and Aranovich and Pattison (1995) in coexisting omphacite–garnet pairs, are 760–820°C for mineral rims and 800–850 for mineral cores. In summary, the HP vein and the host eclogite have been subjected to similar peak metamorphic pressure and temperature conditions, which are around 3.5 GPa at temperatures around 800°C.

Sample set 2: transition from mantle-derived rocks to eclogite

This sample set includes three distinct lithologies (a garnet peridotite, a transition zone, and an eclogite), representing a UHP metamorphic crustal rock that is separated from a mantle-derived rock by a thin transition zone (Fig. 1b). The garnet peridotite (CCSD-2-Gp) consists of olivine, garnet, clinopyroxene, and ilmenite. Chromite and magnetite are accessory phases. Olivine usually shows an interconnected network of serpentinization (Fig. 2b). Exsolution of ilmenite in olivine is a very common feature (Fig. 2c, d). Orthopyroxene has not been observed. The absence of spinel and the preservation of abundant ilmenite exsolutions in olivine grains, while lacking titanoclinohumite, indicate a minimum formation pressure of >5 GPa (Dobrzhinetskaya et al. 1996). Temperatures estimated from Grt–Cpx geothermometers vary from 1,000 to 1,060°C.

The transition zone (CCSD-2-Tr) is about 2 cm thick and contains high modal abundances of coarse-grained omphacite (~60%, up to 3–5 mm in size;) and garnet (~30%, ~1 mm in size), and minor olivine and ilmenite. Chlorite and amphibole are obviously products of fluid/rock interaction (Figs. 2d, e, 3). Ilmenite, chromite, and sulfide phases (FeS) are present in rare cases (Fig. 2f). Very rare orthopyroxene (a few grains on thin-section scale) coexists with amphibole (Fig. 3). The transition zone represents an interface between the garnet peridotite and the eclogite. Based on mineral assemblage, it is part of the eclogite rather than that of the garnet peridotite. The contact between the garnet peridotite and the transition zone is very sharp, indicating no genetic relation between the peridotite and the eclogite (see also Yang et al. 2007). The formation of coarse-grained clinopyroxene (Cpx I) in the transition zone (Fig. 1b) and the occurrence of secondary clinopyroxene (Cpx II, Fig. 3) indicate that eclogite and garnet peridotite came together in close contact under high P–T conditions.

Homogeneous coarse-grained omphacite (Cpx-I, with Na_2O >4 wt%) yields temperatures of 1,015–1,070°C applying the above-mentioned Grt–Cpx thermometers. Application of the Grt–Opx thermometer of Lee and Ganguly (1988) for zoned Opx yields temperatures of 750

Table 2 Pressure–temperature estimate of the investigate samples

Sample	Temperature calculation		Pressure calculation	
	Mineral	*T* (°C, at 2.8 GPa)	Mineral	*P* (GPa, at 800°C)
CCSD-1-Ec	Cpx–Grt (r)	760–820 (EG, KR, AP)	Phen (r)	2.4–2.7 (CA)
	Cpx–Grt(c)	800–850 (EG, KR, AP)	Phen (c)	3.4–3.5 (CA)
CCSD-1-Hv	Cpx(in)–Grt	780–840 (EG, KR, AP)	Phen (r)	2.6–2.9 (CA)
	Cpx–Grt(c)	810–840 (EG, KR, AP)	Phen (m)	3.4–3.5 (CA)
	Qtz–Phen	790–820 (ZH)	Phen (c)	2.5–2.6 (CA)
CCSD-2-Gp	Cpx–Grt (c & r)	960–1050 (EG, KR, AP)	Ilmenite exsolutions in olivine	>5.0 (DO)
CCSD-2-Tr	Cpx(I)–Grt	960–1060 (EG, KR, AP)		
	Cpx(II, c)–Grt	770–890 (EG, KR, AP)		
	Cpx(II, r)–Grt	970–1030 (EG, KR, AP)		
	Opx (c)	700–790 (LG, HA)	Opx (c)	2.5–2.8 (HG)
	Opx (r)	940–960 (LG, HA)	Opx (r)	3.4 (HG)
CCSD-2-Ec	Cpx–Grt (c)	800–900 (EG, KR, AP)		
	Cpx–Grt (r)	910–1000 (EG, KR, AP)		
CCSD-3-Ec	Cpx–Grt	815–840 (EG, KR, AP)		>2.8 (LI)
CCSD-3-Am	Cpx(in)–Grt	800–825 (EG, KR, AP)		>2.8 (LI)
	Am–Grt	760 (RA)		
CCSD-4-Ec	Cpx–Grt	800–850 (EG, KR, AP)		>2.8 (LI)
CCSD-4-Av	Cpx(in)–Grt	800–850 (EG, KR, AP)		>2.8 (LI)
	Qtz–Grt	850 (ZH)		

Abbreviations for applied thermobarometries: *AP* Aranovich and Pattison (1995), *CA* Carswell et al. (1997), *DO*, Dobrzhinetskaya et al. (1996), *EG* Ellis and Green (1979), *KR* Krogh (1988), *HA* Harley (1984), *HG* Harley and Green (1982), *LG* Lee and Ganguly (1988), *LI* Liu et al. (2007), *RA* Ravna (2000), *ZH* Zheng (1993). Other abbreviations: *Am* amphibole, *Cpx* clinopyroxene, *Grt* garnet, *Phen* phengite, *Opx* orthopyroxene, *Qtz* quartz, *c* core, *m* middle, *r* rim; *Cpx (in)* inclusion in garnet

in the core and 790 in the rim rapidly increasing to 960°C at the outermost rim. The corresponding pressure estimates from the Opx–Grt barometer of Harley and Green (1982) are 2.5–2.8 GPa in the core that increase to 3.3 GPa in the rim. The recrystallized Cpx-II with variable but usually <3.5 wt% Na_2O contents is also zoned, giving temperatures around 780°C in the core and increasing to 1,020°C in the rim (Fig. 4). The rimward increase in P–T estimates for the zoned Opx and Cpx-II indicates that the two minerals grew under prograde metamorphic conditions.

Eclogite (CCSD-2-Ec) consists of garnet (~55%), clinopyroxene (~40%), and ilmenite (~5%), similar to the mineral assemblages of the transition zone, but the size of mineral grains is much smaller. No olivine, chlorite, or amphibole has been found in the eclogite. Peak metamorphic temperature conditions calculated for the eclogite are 950–1,020°C, in agreement with those calculated for the garnet peridotite considering the error ranges of the used thermometers.

Sample sets 3 and 4: samples representing retrograde metamorphism

Sample sets 3 and 4 represent coexisting eclogite and retrograde amphibolite, in which the behavior of elements and isotopes during retrograde fluid/rock interaction can be studied. Sample set 3 comprises a relatively fresh (little altered) eclogite (CCSD-3-Ec) and a retrograde amphibolite (CCSD-3-Am) that formed from retrogression of eclogite during exhumation. On the hand specimen scale (about 10 cm), the boundary between the amphibolite and the eclogite is clearly obvious (Fig. 1c). The eclogite (CCSD-3-Ec) consists mainly of garnet, omphacite, and a few percent of rutile. Omphacite close to the boundary to amphibolite shows only slight retrogression at the rim of grains. Amphibolite (CCSD-3-Am) contains low-pressure amphibole and plagioclase with rare garnet and ilmenite but no omphacite. However, abundant omphacite inclusions in rarely preserved garnet point to the same UHP metamorphism as the eclogite. This altogether indicates that fluid addition induced the retrogression of amphibolite from the almost hydroxyl-free precursor assemblage.

Sample set 4 comprises a retrograde amphibolite-vein, being a few centimeters wide, and a well-preserved host eclogite (Fig. 1d). The amphibolite vein (CCSD-4-Av) tends to be filled with symplectite (amphibole + plagioclase) and usually minor quartz, the amount of which increases with the thickness of the vein. The host eclogite (CCSD-4-Ec) consists of omphacite + garnet + quartz + minor rutile.

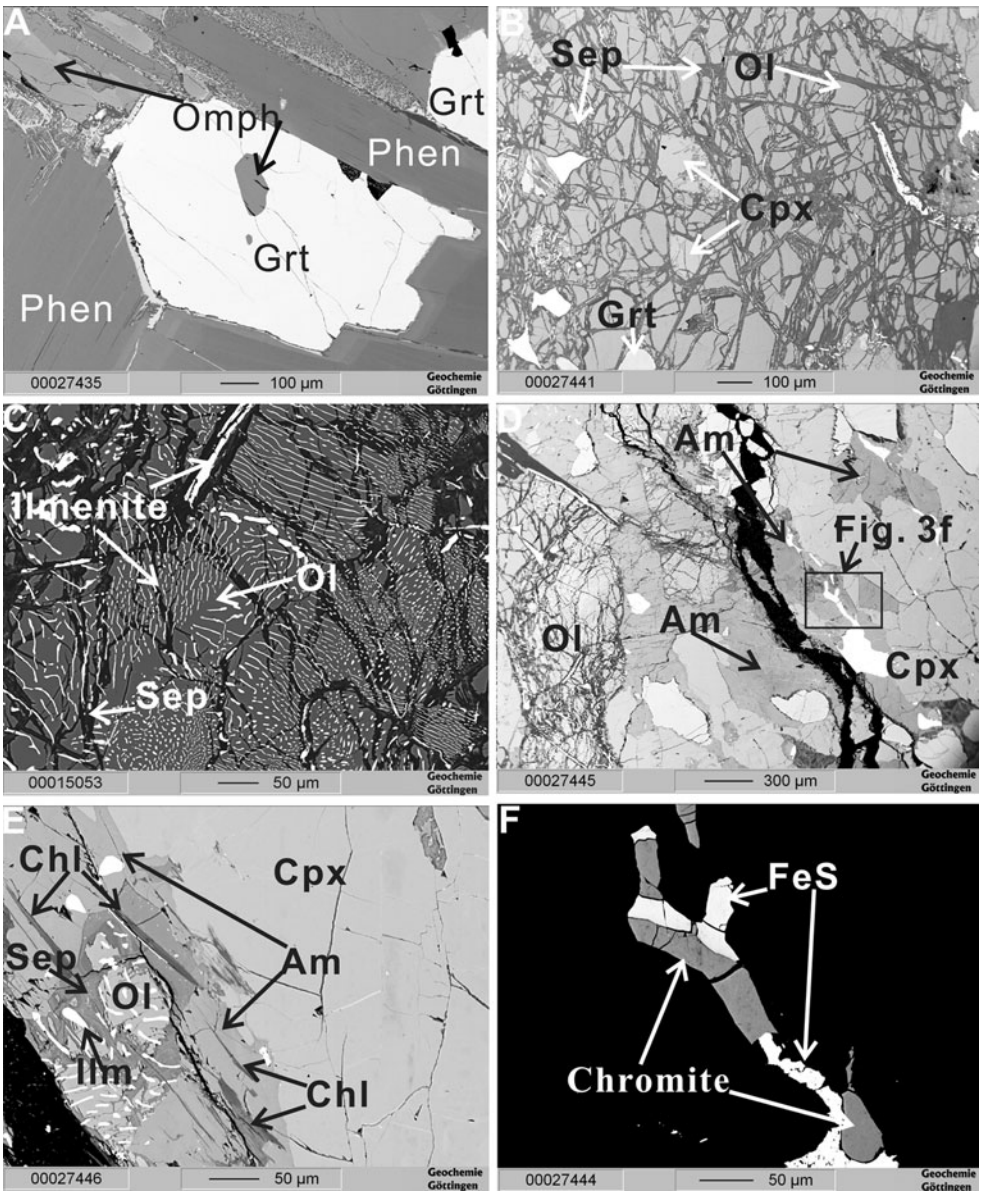

Fig. 2 Backscattered electron (*BSE*) images of investigated samples illustrating petrological features (see text). **a** Coarse-grained phengite, garnet, and omphacite indicate the high-pressure origin of sample CCSD-Hv; slight retrogression can be observed at the rims of phengite and omphacite grains. **b** Olivine is the major mineral phase of the garnet peridotite (*CCSD-2-Gp*); however, retrograded serpentine is also visable. **c** Abundant ilmenite exsolutions in olivine grains refer to very high pressure for the garnet peridotite (Dobrzhinetskaya et al. 1996). **d** and **e** Abundant hydroxyl-bearing minerals occur in the transition zone (*CCSD-2-Tr*) between garnet peridotite and eclogite. **f** Intergrown chromite and sulfide phases (*FeS*) coexisting in the transition zone (*CCSD-2-Tr*)

Peak metamorphic conditions for CCSD-3-Ec were calculated to be 815–840°C at 2.8 GPa using coexisting Grt–Cpx pairs in the matrix (Table 2). Those for retrograde amphibolite (CCSD-3-Am) were estimated to be 810–825°C based on the presence of omphacite inclusions in garnet. For CCSD-4-Ec and CCSD-4-Av, peak metamorphic temperatures are similar, ranging from 800 to 850°C at pressure of 2.8 GPa.

Analytical methods

Major and trace elements

Bulk major elements were determined by X-ray fluorescence (XRF). Glass beads used for analysis were made by mixing with lithium tetraborate as a flux. XRF analysis was undertaken using a Philips PW 1480 automated sequential

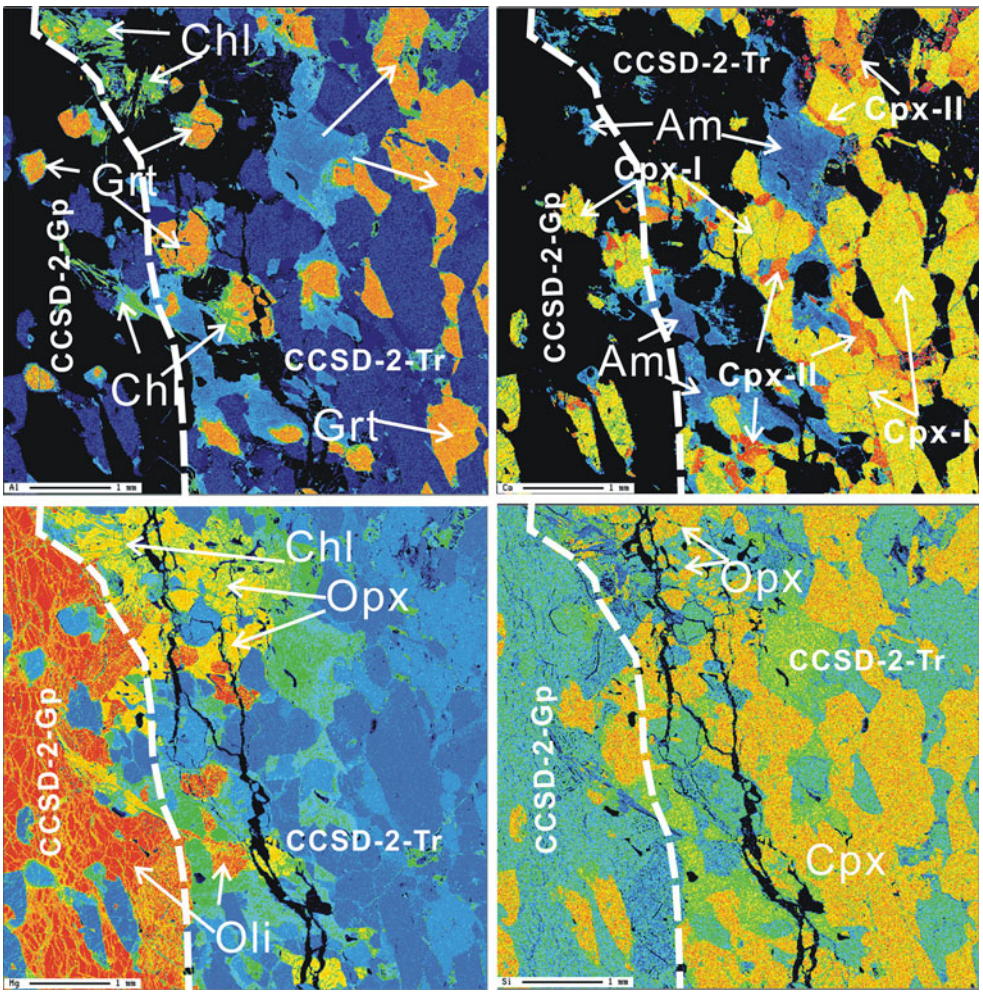

Fig. 3 Semi-quantitative element mapping demonstrating the occurrence of amphibole (*Am*), chlorite (*Chl*), Cpx-I and Cpx-II, and orthopyroxene (*Opx*) in the transition zone (*CCSD-2-Tr*). Cpx-I and Cpx-II in the upper right map refer to primary and secondary clinopyroxene, as defined in the text. Grt, garnet; Oli, olivine

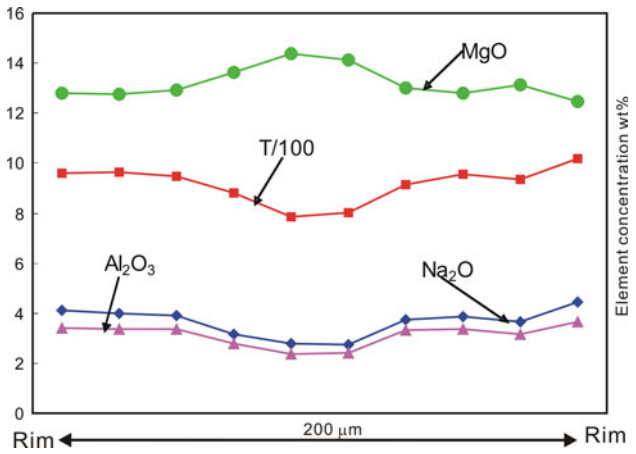

Fig. 4 Compositional zoning profile of a Cpx-II grain from the transition zone between the garnet peridotite and eclogite (sample CCSD-2-Tr), showing increase in metamorphic temperatures (T/100) and pressures (due to rimward Na_2O increase)

spectrometer. Trace elements of bulk rocks were obtained by ICP-MS solution analyses. Samples were digested with HF, $HClO_4$, and HNO_3 at 200°C for a few days in screw-top Teflon vials before evaporation to dryness and dissolution of the residue. Measurements were taken using a Perkin-Elmer DRC II ICP-MS.

Major compositions of minerals were measured on a JXA-8900RL JEOL Superprobe equipped with wavelength-dispersive spectrometers (WDS) and an energy dispersive spectrometer (EDS). Operating conditions were 15.0 kV accelerating voltage, 12 nA beam current, and 5–10 μm electron beam diameter. Standards included were as follows: wollastonite for SiO_2 and CaO, synthetic TiO_2 crystal for TiO_2, synthetic Al_2O_3 crystal for Al_2O_3, synthetic Cr_2O_3 crystal for Cr_2O_3, hematite for FeO, rhodonite for MnO, synthetic MgO crystal for MgO, synthetic NiO crystal for NiO, barite for BaO, albite for Na_2O, and sanidine for K_2O.

Trace element compositions of minerals were acquired by in situ laser ablation inductively coupled plasma mass spectrometry (LA-ICP-MS) both at the University of Science and Technology of China and at the University of Göttingen. Both systems employ a 193-nm ArF Excimer laser coupled to a Perkin-Elmer DRC II ICP-MS. All samples have been prepared as polished thin sections (ca. 2 mm thick). Instrumental background levels were established by a gas blank, that is, analysis of the He–Ar mixed gases with the laser off for 15–20 s. Laser ablation was carried out in a He atmosphere mixed with Ar carrier gas before the plasma torch. ^{29}Si was used as an internal standard; NBS 610 was used as a calibration standard. Reproducibility and accuracy of trace element concentrations were assessed to be better than 10% as checked with both systems. Ablation spots were around 120 μm, with the laser energy of 200 mJ. The ablated aerosol was carried to the ICP source with He gas. Care was taken to perform analyses on crack-free areas of the minerals. The combination of the high-quality optical imaging capabilities of the laser-ablation system and the time-resolved analysis of the ablation signals ensures that mineral inclusions were excluded during measurements.

Li and B concentrations

Li and B concentrations in minerals were analyzed by in situ LA-ICP-MS in which only Li and B as well as a few inner-standard and monitoring elements were included in order to increase the sensitivity during measurements. Li and B concentrations were quantified using the SiO_2 contents of the corresponding electronic probe analysis. The detection limit for Li is about 0.01 μg/g, sufficiently low to investigate Li in the analyzed minerals.

The detection limit of B is not better than 1 μg/g, because of possible surface contamination of the samples—although being carefully cleaned before measurement—and the possibility of B liberation from the sample tubing connecting the laser ablation cell with the ICP-torch (e.g., Lee et al. 2008), Thus, concentrations of B $<$ 1 μg/g in the analyzed minerals are estimates rather than true B contents.

Lithium isotopes

Lithium concentrations and isotope ratios were determined using a ThermoFinnigan MC-ICP MS Neptune at the Research Centre for Earth Sciences in Potsdam (GFZ). About 30–100 mg of powdered sample was dissolved in HNO_3/HF (1:5) and $HClO_4$. Great care was taken to reach complete dissolution, as any residue or precipitate is likely to cause Li isotopic fractionation. Li was separated and purified using a two-step ion-exchange chromatography. The first separation step (HNO_3 in methanol on AG 50 W-8 × 200–400 mesh) followed the setup of Wunder et al. (2006). To remove Na completely, the eluate has been dried again and redissolved in 0.5 ml of 0.5 N HCl in 80% methanol for the second separation (see Jeffcoate et al. 2004). The sample was "washed" with 2 ml of 0.5 N HCl in 80% methanol. Lithium was evaluated from the column with 1 ml of 0.5 N HCl in 80% methanol and with 3.5 ml of 1 N HCl. Complete Li elution was checked by adding and collecting additional 0.5 ml of 1 N HCl. Wash solutions before and after Li elution were analyzed for their Li content. Li loss during the chemical procedure was less than 1%. Each series of Li separation included a NIST 8545 standard solution and reference material JR-2 or JG-2 to check the analytical procedure. Analytical procedure and operating conditions closely correspond to those of Wunder et al. (2006). They showed that the Li blank can reach up to 130 pg but has no influence on the isotopic composition. δ^7Li values are given relative to Li reference material NIST RM 8545 (L-SVEC). The analytical precision and accuracy of δ^7Li were estimated by repeated analysis of reference materials to be 0.19 ± 0.1‰ (1sd) for JG-2 and 4.07 ± 0.34‰ (1sd) for JB-3, which are in the range of published values (Wunder et al. 2006 and references cited there in).

Boron isotopes

Boron concentration was determined on an aliquot of the separated sample using a Varian Vista MPX simultaneous ICP-OES, whereas B isotopic compositions were determined as $Cs_2BO_2^+$ on a Finnigan MAT 262 (Nakano and Nakamura 1998) at the GFZ Potsdam. About 500–1,000 mg of powered sample was fused with K_2CO_3 as described in Kasemann et al. (2001). Separation of boron followed the three-step ion-exchange chromatographic procedure developed by Tonarini et al. (1997). To monitor the analytical procedure, IAEA reference material B5, standard boric acid NBS 951, and a procedure blank were included in each series. All samples with B contents below 0.8 μg/g were analyzed in duplicate or triplicate separate dissolutions. δ^{11}B values of the samples were calculated relative to that of the reference material NBS 951 measured on the same turret. Data given in Table 4 have been corrected to NBS 951 that passed the entire chemical separation procedure having a δ^{11}B value of −0.05 ± 0.23 ‰ (1sd) that reproduces the untreated standard value. The precision and accuracy were estimated based on the analysis of eight independent dissolutions for IAEA standard B5 (basalt) that gave a δ^{11}B value of −4.39 ± 0.53‰ (1sd), which is well in the range of published data (Gonfiantini et al. 2003).

Oxygen isotopes

Oxygen isotopes for minerals were analyzed by "in situ" UV-laser fluorination, whereas those for bulk rocks were measured with a CO_2-laser system in Göttingen. Analytical procedures for UV-laser fluorination have been described in detail in the study by Xiao et al. (2000) and by Wiechert et al. (2002). CO_2-laser measurements for bulk rock were taken on 1–1.5 mg rock powder, which was loaded in a nickel holder with eighteen 2-mm deep holes. After evacuation and heating to ~80°C overnight, the laser was operated at an energy level suitable to transfer the powder lump into a ball, which avoids sample loss during analysis. Afterward, the sample chamber was loaded with 15–25 mbar F_2, and the sample was heated with the CO_2-laser. Oxygen was purified in a way similar to the UV laser method and directly transferred to the Finnigan Delta plus for measurement of $^{18}O/^{16}O$ ratios. Every 10 analyses were bracketed by an internal standard (MORB glass), which has also been run at the beginning and at the end of each measurement day. The routine analytical error based on replicate analysis and standards is better than 0.2‰.

Sr, Nd, and Pb isotopes

Samples were dissolved in concentrated HF at 160°C. Digested samples were dried and taken up in 6 N HCl. Sr and Nd were separated and purified as described in the study by Romer et al. (2005). Sr isotopic composition was determined on a VG54 Sector multi-collector mass spectrometer at GFZ Potsdam. Nd isotopic composition was obtained on a Finnigan MAT 262 multi-collector mass-spectrometer at the same laboratory. $^{87}Sr/^{86}Sr$ and $^{143}Nd/^{144}Nd$ were normalized to $^{86}Sr/^{88}Sr = 0.1194$ and $^{146}Nd/^{144}Nd = 0.7219$, respectively. Analytical uncertainties are given at the 2 σ_m level. Pb was separated using a HBr–HCl ion-exchange procedure (cf. Romer et al. 2005) and analyzed on a Finnigan MAT 262 multi-collector mass-spectrometer. Pb isotope data were corrected for mass discrimination with 0.1% A.M.U. Reproducibility at the 2σ level is better than 0.1%.

Results

Major and trace element compositions of whole rocks are listed in Table 3. Selected mineral microprobe and LA-ICP-MS data are given in Supplementary Table 1 . Li and B elemental and isotopic data are documented in Table 4 and Fig. 6. Oxygen and Sr-Nd-Pb isotopic compositions are documented in Tables 5 and 6, respectively.

Trace elements and Li, B, O isotopes

Sample set 1

Trace element concentrations of the vein and the host eclogite are much higher than those of the primitive mantle, except high-field-strength elements (HFSE), which are relatively depleted (Fig. 5a). Comparison of element concentrations in the vein and the host eclogite demonstrates that CCSD-1-Hv is enriched in components released during prograde dehydration. Thus, incompatible elements Rb, Sr, and Ba, and LREE contents are enriched in CCSD-1-Hv relative to CCSD-1-Ec, indicating that the HP vein is a sink for fluid-mobile elements. By contrast, due to their relative immobility, Nb, Ta, Ti, and HREE are depleted in the vein. In addition, the two samples display very different REE patterns: CCSD-1-Hv has much higher light REE contents but lower heavy REE concentrations than CCSD-1-Ec (Fig. 5a). Major element characteristic and trace element partitioning between the host eclogite and the vein seem to be the result of vein formation during prograde dehydration.

Of special interest are Li and B concentrations and isotope compositions (Table 4). In eclogite, omphacite is the phase with the highest Li concentration ranging from 39.26 to 41.60 μg/g, whereas the B content (0.66 μg/g) is low. Phengite is the main carrier of B in the eclogite, having B concentration from 5.17 to 5.42 μg/g. Garnet is low in both Li and B concentrations, with 0.11 μg/g Li and 0.43 μg/g B. In the HP vein (CCSD-1-Hv), phengite has slightly higher B and Li compared with the host eclogite, with concentrations ranging from 5.47 to 6.13 and 0.64 to 0.73 μg/g, respectively. Eclogite has a δ^7Li of −1.6 ‰ (5.7 μg/g Li), whereas the HP vein (CCSD-1-Hv) has a δ^7Li of 1.2‰ (2.2 μg/g Li) (Table 4; Fig. 6). Boron does not show much difference between the two samples neither in element concentrations nor in isotope compositions (δ^{11}B values are −4.9 and −5.3‰, respectively).

Bulk oxygen isotopic compositions (3.1‰) in the vein are higher than in the host eclogite (1.3‰), resulting from the higher modal abundance of quartz in the vein (Table 5). Homogeneous δ^{18}O values around 2.8–3.0 ‰ have been measured in phengites from both the HP vein and the host eclogite, suggesting that individual phengite grains grew in equilibrium with the same fluid. Coarse-grained quartz from the HP vein shows δ^{18}O values of 4.8–5.1. Estimated temperature of vein formation, using quartz, and phengite oxygen isotope thermometry (Zheng 1993) is around 750°C.

Sample set 2

Garnet peridotite with a depleted heavy rare earth-element (REE) pattern (normalized relative to the PM of Sun and

Table 3 Whole-rock major and trace element data

Sample	CCSD-1-Ec	CCSD-1-Hv	CCSD-2-Gp	CCSD-2-Tr	CCSD-2-Ec	CCSD-3-Ec	CCSD-3-Am	CCSD-4-Ec	CCSD-4-Av
SiO_2	45.4	61.8	40.8	45.5	45.1	41.8	50.9	46.4	53.1
TiO_2	2.19	0.60	0.94	0.49	1.66	5.34	0.91	2.47	2.34
Al_2O_3	18.9	14.8	5.9	11.8	13.3	13.3	15.5	14.5	10.8
$Fe_2O_{3\ (Fetot)}$	12.8	4.4	14.2	13.3	14.7	18.0	9.9	19.1	10.1
MnO	0.25	0.07	0.19	0.27	0.28	0.31	0.15	0.35	0.08
MgO	6.71	4.63	29.6	15.6	13.2	5.55	6.50	4.62	5.80
CaO	8.79	5.87	5.20	9.77	9.76	11.9	8.10	8.76	10.5
Na_2O	2.59	2.83	0.85	1.61	1.60	2.05	4.31	3.09	5.80
K_2O	1.65	3.38	0.04	0.03	0.01	0.02	2.90	0.05	0.03
P_2O_5	0.07	0.41	0.02	0.03	0.02	2.92	0.24	0.48	0.45
Sum (wt%)	99.4	98.7	97.7	98.4	99.7	101.2	99.4	99.8	99.0
Li	5.70	2.20	7.50	12.0	3.60	6.87	4.70	18.00	7.70
Be	0.21	0.29	0.15	0.37	0.34	nd	nd	1.25	0.58
B	1.15	1.77	4.51	1.51	0.91	0.50	1.30	0.40	0.40
Sc	24.7	7.89	9.94	21.4	39.8	14.2	18.3	27.4	43.3
V	146	169	140	254	314	131	205	439	303
Cr	29.0	25.5	1130	968	110	135	7.44	12.2	13.5
Co	17.4	9.27	130	96.4	37.9	26.8	25.4	21.2	28.4
Ni	62.6	37.1	997	873	62.3	64.5	5.16	68.5	74.4
Cu	4.59	1.99	55.7	119	6.39	16.3	17.2	14.0	12.0
Zn	64.1	48.1	86.1	30	32.7	90.3	85.4	111	96.8
Rb	28.6	61.4	0.58	0.43	0.12	0.41	31.3	0.76	1.07
Sr	61.6	189	129	291	279	90.6	412	202	162
Y	9.85	3.27	5.31	15.0	24.2	15.9	12.4	10.5	51.7
Zr	3.65	18.1	13.3	27.3	33.0	5.21	5.96	12.9	43.4
Nb	0.86	0.32	0.46	0.69	1.96	2.96	2.79	5.65	6.50
Mo	0.13	0.15	0.08	0.18	0.13	0.11	0.25	0.51	0.47
Cd	0.05	0.04	0.07	0.14	0.16	0.07	0.10	0.06	0.12
Sn	0.05	0.07	nd	0.33	0.83	0.67	0.37	0.09	0.07
Sb	0.04	nd	0.01	0.01	0.03	0.00	0.02	nd	nd
Cs	0.64	1.41	0.10	0.14	0.05	0.43	0.00	0.03	0.02
Ba	241	662	12.2	50.3	44.2	7.88	354	35.6	21.3
La	0.38	2.39	1.87	4.11	3.98	1.93	18.0	16.7	21.8
Ce	0.98	7.05	5.69	12.7	12.3	4.76	42.1	42.2	52.8
Pr	0.16	1.04	0.89	2.01	1.97	0.67	6.25	5.74	6.90
Nd	1.04	5.75	4.32	9.75	9.8	3.51	31.2	26	30.7
Sm	0.66	1.58	1.10	2.48	2.58	1.09	7.65	6.06	7.17
Eu	0.58	0.75	0.38	0.85	0.93	0.42	2.42	1.67	2.28
Gd	1.25	1.19	1.22	2.86	3.3	1.82	7.61	4.31	7.01
Tb	0.29	0.15	0.18	0.43	0.56	0.39	0.97	0.57	1.40
Dy	1.85	0.70	1.08	2.8	4.13	3.16	5.30	2.51	9.29
Ho	0.40	0.13	0.19	0.54	0.88	0.74	0.93	0.42	1.98
Er	1.12	0.37	0.48	1.46	2.63	2.20	2.27	1.02	5.74
Tm	0.16	0.05	0.06	0.19	0.38	0.32	0.27	0.14	0.84
Yb	0.99	0.34	0.37	1.17	2.49	2.04	1.44	0.84	5.34
Lu	0.15	0.06	0.05	0.16	0.37	0.31	0.20	0.13	0.82
Hf	0.08	0.30	0.42	0.94	1.07	0.18	0.20	0.23	0.66
Ta	0.14	0.04	0.02	0.09	0.26	0.29	0.13	0.37	0.50

Table 3 continued

Sample	CCSD-1-Ec	CCSD-1-Hv	CCSD-2-Gp	CCSD-2-Tr	CCSD-2-Ec	CCSD-3-Ec	CCSD-3-Am	CCSD-4-Ec	CCSD-4-Av
W	0.12	0.13	nd	0.08	0.15	0.03	0.07	0.17	0.22
Tl	0.10	0.24	0.01	nd	nd	0.23	nd	nd	nd
Pb	1.44	3.08	1.58	3.75	3.52	9.60	3.88	2.82	2.38
Th	0.07	0.35	0.03	0.06	0.16	0.28	1.23	1.52	2.43
U	0.03	0.06	0.01	0.01	0.02	0.12	0.45	0.37	0.49

nd not determined

McDonough 1989) has lower REE contents than both eclogite and the transition zone (Fig. 5b). La/Yb ratios for the garnet peridotite, transition zone, and eclogite are 5.1, 3.5, and 1.6, respectively. Garnet peridotite displays a slight LREE enrichment relative to the depleted mantle with a 2–3 times decrease in HREE (Fig. 5b). Eclogite shows PM-normalized REE pattern comparable with N-MORB. Such a pattern is in contrast to that of other eclogites in ultramafic rocks from the Sulu area (Zhang et al. 2009a). The transition zone (CCSD-2-Tr) shows trace element patterns similar to the eclogite or those lying between eclogite and garnet peridotite, except that it is highest in Li but lowest in Ti of the three samples. An Eu anomaly has been observed neither for the garnet peridotite nor for the eclogite. It is also noted that the garnet peridotite and the transition zone have much higher Ni contents (1,115 and 931 μg/g, respectively) than the eclogite (66 μg/g; Table 3). Moreover, the garnet peridotite has a Nb/Ta ratio of 17.8, whereas the eclogite and the transition zone have much lower ratios of 7.2 and 7.1, respectively. In summary, major and trace elements suggest distinct protolith sources for the peridotite and eclogite.

Olivine in garnet peridotite contains 11.35–12.68 μg/g Li but shows a large variation in B ranging from 3.70 to 18.9 μg/g (Table 4). Textural observations and electron microprobe data indicate that olivine and serpentine in the garnet peridotite are often intergrown. After careful LA-ICP-MS spot analysis of pure olivine, we consider the concentration of 3.70 μg/g as reflecting the B concentration of the olivine; the higher concentrations are due to serpentine intergrowth. The rarely found clinopyroxene in the garnet peridotite has 15.30 μg/g Li and 4.12 μg/g B. What is remarkable is that both olivine and clinopyroxene from CCSD-2-Gp have much higher Li and B concentrations than normally found in minerals of fresh orogenic peridotites (1.10–2.73 μg/g,Li and 0.04–0.28 μg/g B for olivine; 1.18–3.90 μg/g Li and 0.05–1.21 μg/g B for Cpx; Ottolini et al. 2004).

Garnet peridotite (CCSD-2-Gp) shows very different δ^{11}B values and B concentrations compared with eclogite (CCSD-2-Ec). CCSD-2-Gp is enriched in B (4.5 μg/g) and ^{11}B (δ^{11}B up to +11.7 ‰) relative to CCSD-2-Ec (0.9 μg/g and −0.1‰, respectively), whereas the transition zone (CCSD-2-Tr) has an intermediate composition, with B = 1.5 μg/g and δ^{11}B = + 5.8‰ (Table 4, Fig. 6). Minor serpentine is intergrown with olivine in the garnet peridotite (Fig. 2b). Thus, the measured B-content of olivine in the garnet peridotite may be biassed by the presence of serpentine. To distinguish the B content of olivine from that of the serpentine, we checked after the LA-ICP-MS measurements, the analyzed spots by electron microprobe analyses. Contents of ∼3.70 μg/g B were obtained for pure olivine, whereas up to 18.9 μg/g B was found when ∼90% serpentine was involved. Considering the high modal abundance of olivine and the much lower one of the serpentine, we suggest that olivine is the major B carrier phase, which accounts for more than 60% of the total B inventory of the garnet peridotite. Therefore, the systematic variation in B content and δ^{11}B probably reflects fluid addition of B from the eclogite to the contact garnet peridotite. In contrast to the large variation of B isotopes, Li isotope variations in the three samples are minor, being around 2 ‰ slightly lower than those for fresh MORB (Chan et al. 1992; Elliott et al. 2002; Tomascak et al. 1999).

Minerals from the garnet peridotite (CCSD-2-Gp) have δ^{18}O ranging from 2.9 to 3.6 for olivine, 3.6–4.0 for clinopyroxene, and 3.6–3.9 for garnet (Table 5), significantly lower than those from unaltered mantle peridotite (e.g., Chazot et al. 1997). Garnets and clinopyroxene from the transition zone show δ^{18}O values of 3.1–3.3 and 3.3–3.6, whereas those from the eclogite have values of 2.7–3.1 and 3.2–3.4, respectively.

Sample sets 3 and 4

Within sample set 3, retrograde amphibolite (CCSD-3-Am) has much higher fluid-mobile element concentrations (Rb, Ba, Sr, 4–80 times higher) than eclogite (CCSD-3-Ec; Table 3 and Fig. 5c) and displays much higher light REE but similar heavy REE compared with the eclogite, despite the much higher garnet abundance in the latter (Fig. 5c). A characteristic feature of sample set 4 is that PM-normalized

Table 4 Li and B elemental and isotopic data of CCSD UHP metamorphic rocks

Sample[a]	Whole rock				Mineral phase							
	$Li^{a,b}$	δ^7Li	B	$\delta^{11}B^c$	Garnet		Clinopyroxene		Phengite		Olivine[e]	
					Li^d	B	Li	B	Li	B	Li	B
CCSD-1-Ec	5.7	−1.6 ± 1.0	1.2	3.1 ± 0.7 (4)	0.11 (3)	0.43 (3)	40.35 (4)	0.66 (4)	0.66 (5)	5.6 (5)		
CCSD-1-Hv	2.2	1.2 ± 0.5	1.8	0.9 ± 0.5 (3)	0.13(2)	0.35 (2)	6.73 (1)	1.20 (1)	0.71 (6)	5.9 (6)		
CCSD-2-Gp	7.5	2.4 ± 0.1	4.5	11.7 ± 0.5			15.32 (2)	4.21 (2)			11.8 (5)	3.7 (1)
CCSD-2-Tr	12	1.8 ± 0.1	1.5	5.8 ± 0.5	3.3 (2)	0.34 (2)	16.66(2)	0.9 (2)				
CCSD-2-Ec	3.6	2.5 ± 0.1	0.9	−0.1 ± 0.5	0.78(1)	0.53(1)	13.5 2(2)	0.59 (2)				
CCSD-3-Ec	14	−6.5 ± 0.1	0.5	−9.3 ± 0.5 (2)								
CCSD-3-Am	9.7	0.9 ± 0.2	1.3	−1.1 ± 1.4 (2)								
CCSD-4-Ec	18	−6.9 ± 0.2	0.4	−4.9 ± 1.6 (2)								
CCSD-4-Av	7.7	−0.4 ± 0.3	0.4	−5.3 ± 0.7 (3)								

[a] Elemental concentration is in ppm. The contents and isotopic compositions of Li and B were determined on separate aliquots from the same sample

[b] Whole-rock Li and B contents determined for the optimal setup of the ion-exchange procedure were used in the preparation of the samples for the determination of isotope ratios

[c] $\delta^{11}B$ represents the mean of n (indicated in the brackets) separately dissolved aliquots

[d] Concentrations represent an average value of n (indicated in the brackets) measurements

[e] Due to the intergrowth between olivine and serpentine, Li and B analyses of olivine in the garnet peridotite were compromised by the presence of serpentine. We checked the analyzed spots with electron microprobe after in situ LA-ICP-MS measurements and found that value of 3.70 ppm B was carried on a pure olivine grain whereas the higher values from 4.12 to 18.88 ppm involved variable amounts of serpentine, with 90% serpentine for the highest value of 18.88. Therefore, we take 3.70 ppm as the B concentration in the olivine

Table 5 Oxygen isotopic compositions of bulk and major mineral phases in UHP rocks from the CCSD, Sulu, China

Sample	Whole rock[a]	Quartz	Garnet	Clinopyroxene	Phengite	Olivine
CCSD-1-Ec	1.26 (*1.6*[b])		1.6–1.9 (4)	1.9–2.2	2.8–3.0 (3)	
CCSD-1-Hv	3.07 (*3.0*[b])	4.8–5.1 (5)[c]	1.9 (1)	2.4 (1)	2.8–3.2 (7)	
CCSD-2-Gp	3.89		3.6–3.9 (2)	3.6–4.0 (3)		2.9–3.6(5)
CCSD-2-Tr	3.41		3.1–3.3 (3)	3.3–3.6 (6)		
CCSD-2-Ec	3.08		2.7–3.1 (3)	3.2–3.4 (3)		
CCSD-3-Ec	1.21					
CCSD-3-Am	2.52					
CCSD-4-Ec	1.68		1.7–1.8 (2)	2.0–2.1 (2)		
CCSD-4;Av	1.79	4.2–4.4 (4)	1.7–1.9 (3)			

[a] Values reported in the conventional $\delta^{18}O$ notation relative to the Standard Mean Ocean Water (SMOW)

[b] Value estimated from mineral oxygen isotopic compositions and modal abundance

[c] Number in bracket indicates the times of analyses

Table 6 Sr-Nd-Pb isotope data of investigated samples from CCSD, Sulu, China[a]

Sample	$^{87}Sr/^{86}Sr$ ($\pm 2\ \sigma_m$)[b]		$^{143}Nd/^{144}Nd$ ($\pm 2\ \sigma_m$)[c]	ε_{Nd}	$^{206}Pb/^{204}Pb$[d]		$^{207}Pb/^{204}Pb$		$^{208}Pb/^{204}Pb$	
	Measured	(T)	Measured	(T)	Measured	(T)	Measured	(T)	Measured	(T)
CCSD-1-Ec	0.708847 ± 7	0.70441	0.512794 ± 9	−2.7	17.402	17.35	15.492	15.49	37.906	37.87
CCSD-1-Hv	0.707813 ± 10	0.70471	0.512499 ± 5	−1.8	17.329	17.28	15.433	15.43	37.740	37.65
CCSD-2-Gp	0.705165 ± 10	0.70512	0.512364 ± 7	−4.1	16.904	16.89	15.392	15.39	37.313	37.30
CCSD-2-Tr	0.705114 ± 11	0.70510	0.512355 ± 5	−4.2	16.826	16.82	15.370	15.37	37.255	37.24
CCSD-2-Ec	0.705078 ± 7	0.70507	0.512417 ± 8	−3.3	16.804	16.79	15.371	15.37	37.268	37.26
CCSD-3-Ec	0.706328 ± 10	0.70632	0.512443 ± 5	−2.3	17.330	17.22	15.435	15.43	37.828	37.73
CCSD-3-Am	0.711226 ± 12	0.70793	0.512477 ± 5	−2.9	17.305	17.23	15.440	15.44	37.715	37.66
CCSD-4-Ec[e]	0.706321 ± 7	0.70626	0.512350 ± 5	−3.9	17.809	17.32	15.486	15.46	38.437	37.65
	0.706358 ± 7	0.70630	0.512356 ± 5	−3.8						
CCSD-4-Av[e]	0.706292 ± 10	0.70626	0.512366 ± 5	−3.6	17.592	17.33	15.446	15.43	37.925	37.51
	0.706295 ± 7	0.70626	0.512360 ± 5	−3.7						

[a] The isotopic compositions of Sr, Nd, and Pb are from the same aliquots. The initial isotopic compositions were determined for $T = 240$ Ma, which represents the time of the collision between the North China and Yangtze plates (Li et al. 1993). For analytical details, see Romer et al. (2005)

[b] Analyzed using dynamic multicollection using a VG Sector 54-30 TIMS. Values are normalized to $^{86}Sr/^{88}Sr = 0.1194$

[c] Analyzed using dynamic multicollection using a MAT 262 TIMS. Values normalized to $^{146}Nd/^{144}Nd = 0.7219$

[d] Measured ratios corrected for mass fractionation with 0.1%/a.m.u. as determined from the repeated measurement of NBS 981 Pb reference material. Reproducibility is better than 0.1%

[e] Sr and Nd isotopic compositions of samples CCSD-4-Ec and CCSD-4-Av were determined on separate dissolutions of aliquots from the same powder

trace element patterns (Fig. 5d) are generally very similar for eclogite and amphibolite, excluding HREE, which is due to the higher garnet abundance in the host eclogite.

Sample CCSD-3-Ec (eclogite) has low B concentration (0.5 μg/g) and a $\delta^{11}B$ value of −9.3‰, whereas the retrograde amphibolite (CCSD-3-Am) has higher B content (1.3 μg/g) and a heavier $\delta^{11}B$ value (−1.1‰) (Table 4; Fig. 6). This suggests that B was added by fluids to the amphibolite, and that, if the precursor of the amphibolite had a similar B isotopic composition as the eclogite, the fluid must have had strongly positive $\delta^{11}B$ values. Significant elemental and isotopic variations are also observed for Li, with $\delta^{7}Li$ of −6.5‰ (14 μg/g) and of +0.9‰ (9.7 μg/g) in CCSD-3-Ec and CCSD-3-Am, respectively (Table 4; Fig. 6).

For sample set 4, B concentration and isotopic composition are very similar, indicating limited B addition during the formation of the retrograde amphibolite (CCSD-4-Av). However, Li concentration and isotopic composition vary between CCSD-4-Ec and CCSD-4-Av. The former has Li

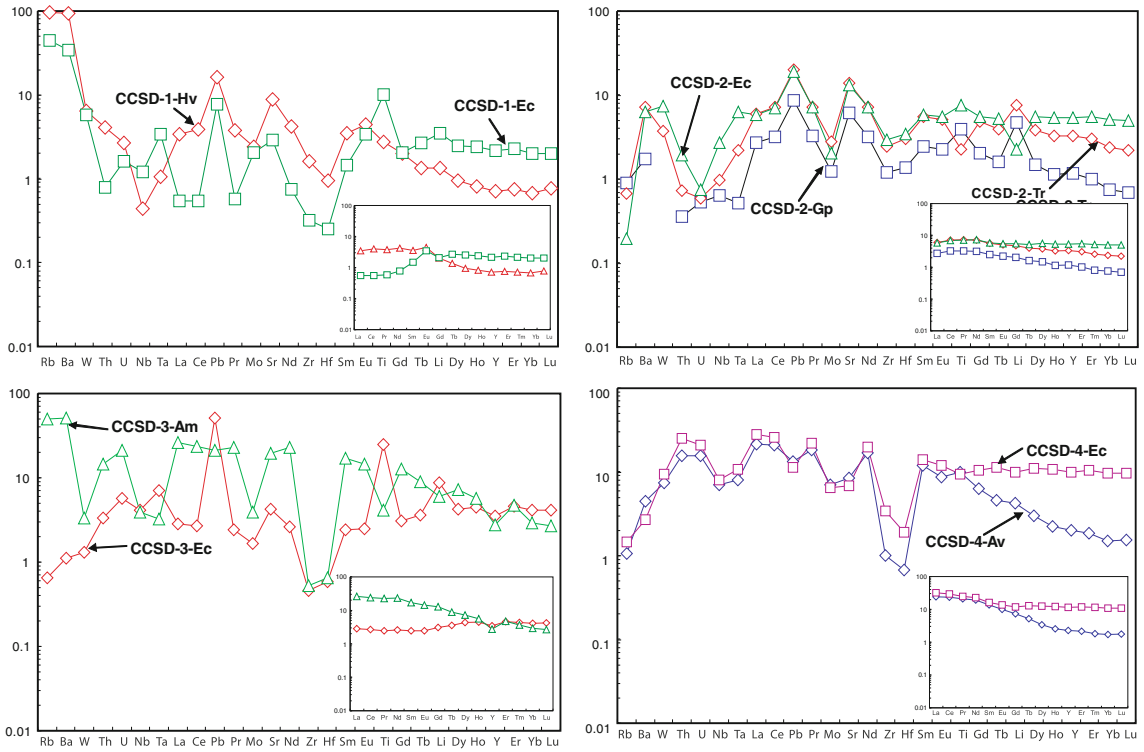

Fig. 5 Primitive mantle-normalized bulk rock trace element patterns for selected samples from the CCSD. Normalized values for primitive mantle are from Sun and McDonough (1989)

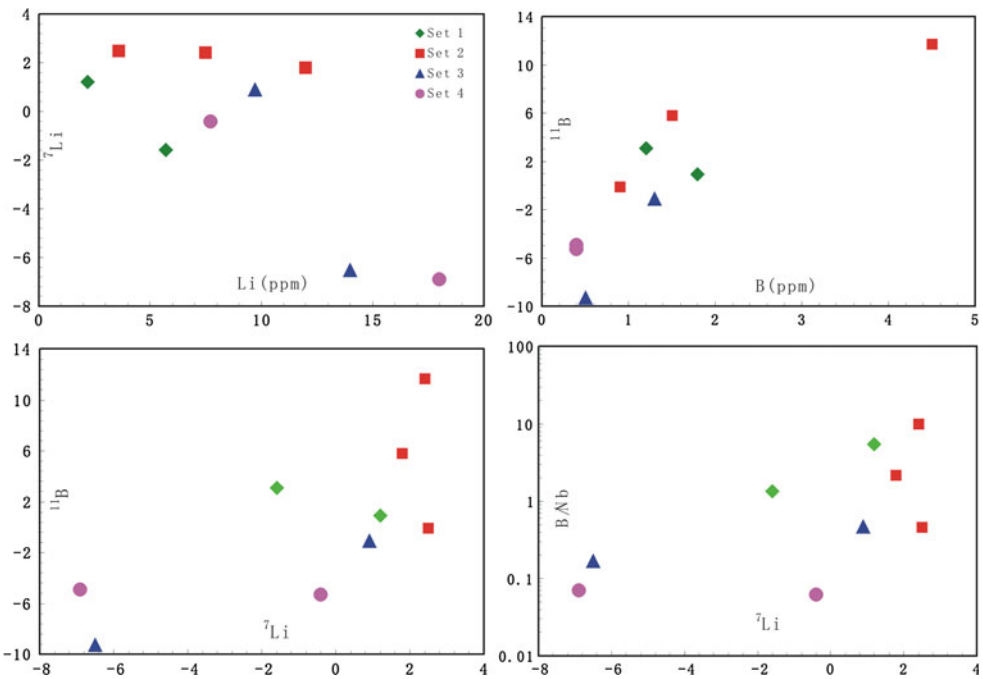

Fig. 6 δ^7Li versus Li (**a**), δ^{11}B versus B (**b**), δ^7Li versus δ^{11}B (**c**), and B/Nb versus δ^7Li (**d**) plots for investigated UHP metamorphic rocks from the CCSD

content of 18 μg/g and a δ^7Li value of −6.9 ‰, whereas the latter has 7.7 μg/g Li and a δ^7Li value of −0.4 ‰, suggesting strong Li isotope fractionation between eclogite and amphibolite (Table 4; Fig. 6).

Garnets from both CCSD-4-Ec and CCSD-4-Av have very similar δ^{18}O values of 1.7–1.9, whereas quartz in CCSD-4-Av has δ^{18}O values of 4.2–4.4 (Table 5). Coexisting garnet–quartz pairs (Zheng 1993) in the vein yield

equilibrium temperatures of about 850°C, indicating oxygen isotope equilibrium under high-temperature conditions.

Whole-rock Sr-Nd-Pb isotopes

The Sr-Nd-Pb isotopic data are summarized in Table 6. Sr and Nd isotopic compositions show large $^{87}Sr/^{86}Sr_{(T\,=\,240Ma)}$ variations ranging from 0.70441 to 0.70793 and low ε_{Nd} values from −2.3 to −4.2 at 240 Ma, representing the age before subduction (Li et al. 2000). In a $^{87}Sr/^{86}Sr_{(240\ Ma)}$ versus ε_{Nd} plot (not shown), all investigated samples coincide with eclogites from the Dabie–Sulu area, which are characterized by relatively enriched Sr and Nd isotopic compositions (John 1998; Wawrzenitz et al. 2006). The sample CCSD-1-Ec shows a slight difference in measured but similar initial (calculated for 240 Ma) $^{87}Sr/^{86}Sr$ ratios and ε_{Nd} values to the HP vein (CCSD-1-Hv), indicating that vein-forming fluids were probably derived from the eclogite (e.g., Becker et al. 1999).

The three samples from the coexisting garnet peridotite and eclogite have similar initial Sr and Pb isotopic compositions, but slightly different initial Nd isotopic compositions (Table 6). A high $^{87}Sr/^{86}Sr$ ratio and a negative initial ε_{Nd} value in the garnet peridotite (CCSD-2-Gp) may reflect input from subducted eclogites (CCSD-2-Ec).

As typical for eclogites of the Dabie–Sulu area, all analyzed samples have unusually unradiogenic Pb isotopic compositions due to a marked reduction in their Th/Pb and U/Pb ratios during a Palaeoproterozoic or Archean high-grade metamorphic event (Li et al. 2003; Wawrzenitz et al. 2006). In $^{207}Pb/^{204}Pb_{(T)}$ versus $^{206}Pb/^{204}Pb_{(T)}$ and $^{208}Pb/^{204}Pb_{(T)}$ versus $^{206}Pb/^{204}Pb_{(T)}$ ($T = 240$ Ma) diagrams (not shown), coexisting garnet peridotite and eclogite fall in the field of post-collisional mafic-ultramafic intrusive (PCMI) rocks (Li et al. 2009). The similarity in unradiogenic Pb isotopic compositions of eclogite and peridotite (Table 6) suggests that the Pb budget of the garnet peridotite is dominated by eclogite-derived Pb,

Retrogressed amphibolite and eclogite, CCSD-4-Ec and CCSD-4-Av, have very similar initial Sr and Nd isotopic compositions. On the other hand, significant differences in Sr isotopes are observed between CCSD-3-Ec and CCSD-3-Am (Table 6), which suggest Sr input from the retrograde fluid. The very similar initial Nd and Pb isotopic compositions of CCSD-3-Ec and CCSD-3-Am suggest that the rocks had the same precursor lithology.

Discussion

The 4 sets of samples characterize 3 different temperature–pressure conditions in a continental subduction-related environment. We will discuss the 3 metamorphic settings: (i) element transport during prograde dehydration conditions, (ii) material exchange among mantle- and slab-derived rocks and, (iii) fluid/rock interactions during retrograde metamorphism. Of special importance for the discussion is the role of Li and B during the various metamorphic stages.

Element transport during prograde dehydration

Before we discuss the evidence for element transport under prograde dehydration, we have to consider whether the vein represents segregated partial melt. Peak metamorphic conditions of the investigated HP vein up to ~800°C and up to at least 3.5 GPa, close to the water-saturated solidus of eclogite (Schmidt et al. 2004b), should favor melting. However, the preservation of quartz and phengite in the residual eclogite suggests that the HP vein cannot be a melt phase from the host eclogite. In particular, the sharp contact between the vein and the eclogite speaks against partial melting. Furthermore, the SiO_2 content in the vein (61 wt%) is too low for a partial melt of a mafic rock at eclogite facies conditions (Rapp and Watson 1995). In addition, the enrichment of phengite, coarse-grained quartz, and amphibole in the vein suggests that the vein most likely was deposited from silicate-rich fluids (Kessel et al. 2005; Schmidt et al. 2004a).

Phengite occurs in both the HP vein and the host eclogite. Its major element (such as Si and K) and trace element composition (Rb and REE) is comparable in both phases. Calculations based on available thermobarometers yield similar peak metamorphic pressures of 3.4–3.5 GPa and temperatures of ~800°C for both the vein and the host eclogite, which indicates that phengites have been subject to the same P–T evolution. However, phengite from the HP vein has much higher Sr and Ba and slightly higher Eu concentrations relative to the host eclogite, indicating that fluid-mobile trace elements have been transported from the host eclogite to the HP vein.

As shown in Fig. 7, SiO_2 content of phengite from CCSD-1-Hv is negatively correlated with BaO content: the phengite core has low Si and high Ba contents, whereas the rim shows higher Si but lower Ba concentrations. Few analyzed spots from the outermost phengite rim have both low SiO_2 and BaO contents, which may indicate that the rims had originally higher Si contents being lowered during retrogression. As mineral cores record earlier growth histories than rims, the increase in Si from core to rim indicates increasing pressures during phengite growth (e.g., Massone and Schreyer 1987). Since Ba is a typical fluid-related element, the correlation suggests that the phengite cores equilibrated with a Ba-rich fluid. Overall, these observations suggest that phengites in the vein formed under a typical subduction dehydration environment.

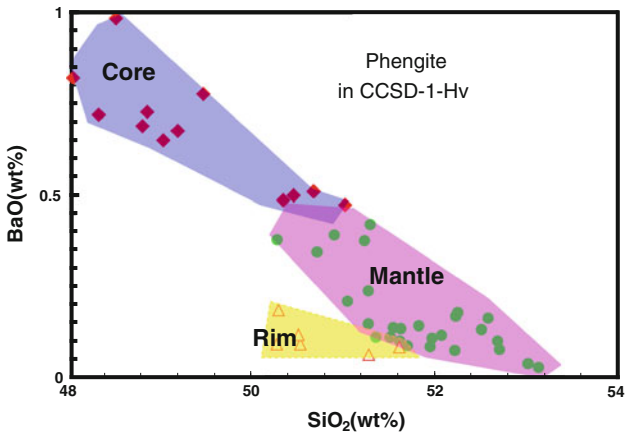

Fig. 7 SiO_2 versus BaO profiles through coarse-grained phengite from the high-pressure vein (*CCSD-1-Hv*), divided into core (*blue*), mantle (*pink*), and rim (*yellow*) areas

Garnet and omphacite from the HP vein have comparable middle to heavy REE contents but higher Rb, Sr, Ba, and LREE concentrations relative to the host eclogite (Supplementary Table 1) that may imply material transport from the host eclogite into the vein. Whole-rock oxygen isotope calculation based on mineral modal abundances and measured mineral $\delta^{18}O$ values yields a bulk value of 3.0 ‰ for the HP vein and 1.6 ‰ for the host eclogite. This difference is due to the different modal abundance of quartz ($\delta^{18}O = \sim 5.0$). Therefore, trace element, mineralogical and oxygen isotope data suggest that the fluid responsible for the formation of the HP vein originates from the surrounding eclogite. Comparing the volume of the vein with that of the host eclogite, fluids forming the vein must not necessarily be derived from the immediate host rock, but instead, may originate from a larger portion of surrounding dehydrated eclogites.

As Li and B are fluid-mobile elements (Marschall et al. 2006), they will be expelled during dehydration causing isotope fractionation. Since the heavy isotopes ^{7}Li and ^{11}B preferentially enrich in the fluid phase (Benton et al. 2004; Benton et al. 2001), the deposited minerals in the HP vein should be depleted in ^{7}Li and ^{11}B. However, compared with the host eclogite, the HP vein has higher $\delta^{7}Li$ but lower $\delta^{11}B$ values, reflecting possibly different behavior of the two elements during vein formation. Apparently, a major part of the fluid and some of it contained Li and B that are mobile at relatively low P–T conditions would migrate away from the vein-forming fluid, lowering significantly the element concentrations and probably also changing the isotopic compositions in the vein minerals. The Li and B elemental and isotopic features of the vein will thus not reflect the budget of the dehydrated fluids but that of a residue after a series of complex processes.

Material and fluid exchange between mantle- and slab-derived rocks

Fluids released from subducting oceanic crust (Bebout et al. 1993; Bebout and Barton 2002; King et al. 2003; Kohler et al. 2009) or from continental crust (Marocchi et al. 2007, 2009; Zhang et al. 2007) may transfer large amounts of volatiles and trace elements to the overlying mantle wedge. The metasomatic mineral assemblage at the interface between peridotite and eclogite represents one rare example in orogenic peridotite that has been affected by UHP metamorphic conditions. The presence of amphibole and chlorite in the transition zone between garnet peridotite and eclogite is strong evidence for a metasomatic process in which fluids have been added to garnet peridotite. Before we discuss this topic in more detail, we have to address the question: whether garnet peridotite and eclogite are rocks from different sources brought together during slab subduction or alternatively products of differentiation, i.e., cumulates of an intruded ultramafic body.

Primitive-mantle-like REE patterns (Fig. 5b) in the garnet peridotite (CCSD-2-Gp) favor a mantle origin for the rock. As mentioned, the investigated garnet peridotite has been collected from the drill hole ZK 703 that is ~80 m away from the main hole of the CCSD that penetrates the same ultramafic rock body (Xiao et al. 2006). Based on a general petrochemical study on the recovered garnet peridotite from the CCSD main hole, Yang et al. (2007) argued that garnet peridotite and interlayered eclogite should derive from different sources. Such a conclusion is supported by different formation ages of the two rock types: peridotites have protolith ages of 346–461 Ma (Yang et al. 2007), whereas eclogites interlayered with the peridotite have protolith ages >600 Ma (Zhang et al. 2009b). Further support is obtained from mineral chemistries at the interface between eclogite and garnet peridotite. As shown in Fig. 3, in the transition zone, two compositionally different Cpx grains (Cpx-I and Cpx-II) may occur, with Cpx-II as overgrowths at the rim of Cpx-I or as individual grains showing compositional core-rim zoning. Profiles through Cpx-II grains show decreasing MgO and CaO contents whereas jadeite component and Al_2O_3 increase from core to rim of the grain (Fig. 4). Assuming chemical equilibrium between the rims of coexisting Cpx-II and garnet, Cpx–Grt thermometry of Aranovich and Pattison (1995) yields temperatures of 960–1,020°C at the rim and 780–800°C at the core for Cpx-II (Table 2; Fig. 4). Such zoning patterns—also observed in orthopyroxene grains—may have been obtained during prograde metamorphism. The zoned Cpx-II and Opx grains indicate near-peak formation conditions, suggesting that coexisting amphibole and sulfide (FeS) in the transition zone (Fig. 2f) might have formed under similar P–T conditions.

In summary, the sharp contact between the two rock types (Fig. 2b), the presence of hydroxyl-bearing minerals along the interface, a >10% bulk MgO difference between peridotite and eclogite, and the different protolith ages confirm that garnet peridotite and eclogite represent rocks from different sources that have been brought together during slab subduction. Numerical modeling by Gerya and Stöckhert (2006) has shown that rocks from different lithospheric levels, following different P–T paths, can be amalgamated through a "subduction channel." The rimward temperature and pressure increases in Opx and Cpx-II in the transition zone suggest that the garnet peridotite was brought together with the down-going eclogite before peak metamorphism.

The growth of new minerals such as amphibole, chlorite, and Cpx II strongly suggests formation by hydrous fluids rich in silicate component. Comparison of mantle-normalized trace element patterns of garnet and clinopyroxene in garnet peridotite and in eclogite shows the characteristic features of associated subduction zone fluids, which is also documented by the overall enrichment of Rb, Ba, and Sr in the garnet peridotite minerals (Supplementary Table 1). Garnet peridotite (CCSD-2-Gp) has bulk Li and B contents of 7.5 and 4.5 μg/g, respectively, which are considerably higher than previously reported values for the depleted mantle (typically <2 and <1 μg/g, respectively) (Palmer and Swihart 1996; Paquin and Altherr 2002; Paquin et al. 2004; Sun and McDonough 1989). Studies on oceanic peridotite showed that B is generally enriched, whereas Li is depleted in serpentine minerals and serpentinite during alteration (e.g., Niu 2004; Vils et al. 2008). As the garnet peridotite is partially serpentinized, it might be argued that the B enrichment results from the late serpentinization. However, in situ measurement of B and Li concentrations indicates that primary olivine and clinopyroxene have B contents up to 3.7 and 4.1 μg/g, respectively, which are much higher than those from depleted mantle (Ottolini et al. 2004; Salters and Stracke 2004). The B enrichment, thus, seems to be a primary feature of the rock. As shown by the narrow range of Li concentrations in the analyzed spots, the slight serpentinization does not affect significantly the Li concentrations in the primary mineral phases. Therefore, B and probably Li enrichment in the garnet peridotite results from metasomatic fluids released during the dehydration of the subducting slab (represented by the eclogite).

In contrast to earlier suggestions that B cannot reach depths greater than the volcanic roots of arcs (Ishikawa and Nakamura 1994; Morris et al. 1990), the present study indicates that a relatively large amount of crustal B and Li can be recycled to mantle depths. This is in line with You et al. (1993), who estimated that possibly less than 30% of slab B input from subducted sediments and altered oceanic crust is brought back to the surface in arcs. This is also consistent with the modeling results by Marschall et al. (2007b) who suggested that about 55% Li and ~37% B in K_2O-bearing MORB may retain in the rocks up to eclogite-facies metamorphism. Therefore, crustal-derived Li and B may contribute significantly to the Li and B budget of the mantle.

With respect to isotopes, Li shows a small isotopic fractionation from 1.8 to 2.5 ‰ relative to typical mantle values (Chan et al. 1992; Elliott et al. 2002, 2004; Tomascak 2004), whereas B displays significant isotopic fractionation along the profile from eclogite to garnet peridotite, with $\delta^{11}B$ values of −0.1 for eclogite to 5.8 for the transition zone and to 11.7 for garnet peridotite (Table 4; Fig. 6). It is unlikely that the B isotope fractionation results from late-stage, low-temperature processes, because olivine and clinopyroxene are the major B-bearing phases (Table 4) and because the two rocks behaved structurally coherent during exhumation. Any fluid/rock interaction at low temperatures is likely to affect both the Li and B isotope systems. The contrasting behavior of Li and B under mantle conditions may be due to that: (i) Li isotope fractionations are smaller than B (James et al. 2003; Kisakurek et al. 2004; Rudnick et al. 2004; Zack et al. 2003); (ii) fluids released from UHP eclogites may have much lower eclogite/fluid partition coefficients for B than for Li (Kessel et al. 2005); and (iii) the whole-rock budget of Li and B is controlled by different minerals, i.e., B is preferentially hosted in phengite (Domanik et al. 1993; Marschall et al. 2006; Wunder et al. 2005; this study), whereas Li is predominantly hosted in clinopyroxene and olivine (Marschall et al. 2006; Seitz et al. 2004; Woodland et al. 2002; Zack et al. 2002). Thus, the small range of δ^7Li values may indicate an exchange at very high temperatures.

Oxygen isotope data are in line with these arguments. The small increase in $\delta^{18}O$ values from 3.1 for the eclogite to 3.3 for the transition zone and to 3.9 for the garnet peridotite indicates an addition of fluids from the eclogite to the garnet peridotite, because the isotopic front of the fluids from the former (with $\delta^{18}O$ of ~3.1‰) to the latter (with $\delta^{18}O$ >3.9‰) will become less steep with increasing distance from the eclogite. Those fluids are released from the ecogite is also documented by the occurrence of chlorite and amphibole in the transition zone between the two rocks.

Fluid/rock interaction during exhumation: origin(s) of the retrograde fluids

With respect to the source of fluid(s) that caused the formation of retrograde amphibolite in the Dabie–Sulu area, numerous studies ascribed the origin of retrogression to

deep infiltration of external fluids (Baker et al. 1997; Xiao et al. 2000; Yui et al. 1997), while others argued that the liberation of internal fluids from the rocks themselves could be an important source (Chen et al. 2007; Li et al. 2004; Zheng 2009; Zheng et al. 2007). In the present case, an external fluid source can explain the very different fluid-mobile element budgets as well as oxygen isotopic compositions in samples CCSD-3-Ec and CCSD-3-Am; however, internal fluids released by the exsolution of structural water from nominally anhydrous minerals after peak metamorphism may provide sufficient amounts of aqueous fluid for amphibolite-facies retrogression (e.g., Li et al. 2004; Chen et al. 2007; Zheng et al. 2007; for review, see Zheng 2009) in CCSD-4-Av. This is indicated by the observation that CCSD-4-Av has a 40% higher modal abundance of water-rich omphacite than CCSD-4-Ec (see below). Thus, both external and internal fluids may contribute to the retrogression of the UHP metamorphic rocks.

The investigated retrograde amphibolite samples (CCSD-3-Am and CCSD-4-Av) may have different fluid sources, as indicated by their different major components and trace elements characteristics. The markedly higher contents in Fe, Ti, and P in CCSD-3-Ec may be due to cumulate ilmenite and apatite in the precursor. The 4–80 times higher fluid-mobile element concentrations of Rb, Ba, and Sr in CCSD-3-Am relative to CCSD-3-Ec suggest that a substantial volume of these elements must have been added from external fluids (Fig. 5c), consistent with the occurrence of fractures within the amphibolite (Fig. 1c). The fact that no structural break is observed between CCSD-3-Ec and CCSD-3-Am implies that the mineralogical difference between the two samples largely reflects the contrasting extent of retrograde overprint.

On the other hand, samples CCSD-4-Av (amphibolite-vein) and CCSD-4-Ec (host eclogite) are similar in TiO_2, MgO, and P_2O_5 contents. Using bulk rock major element data and measured compositions of omphacite and garnet, an eclogite composed of 88% omphacite and 12% garnet is consistent with sample CCSD-4-Av, whereas an eclogite with 48% omphacite and 52% garnet may explain the concentrations of major elements in CCSD-4-Ec (Fig. 8). The presence of about 2% rutile in garnet and omphacite from CCSD-4-Ec explains the similar TiO_2 contents in both samples. Furthermore, the two samples are also very similar in most trace element concentrations (Table 3; Fig. 5d), including the fluid-mobile elements, except the HREE, which are much higher in the host eclogite (Fig. 5d). Therefore, the formation of CCSD-4-AV results from retrogression of omphacite to amphibole in an omphacite-enriched layer, as omphacite may have much more structural water than garnet (Chen et al. 2007) and react easier with fluid relative to garnet.

This model again is consistent with oxygen isotope data. For sample set CCSD-3, eclogite CCSD-3-Ec has a bulk $\delta^{18}O$ value of 1.3, whereas the retrograde amphibolite CCSD-3-Am has a $\delta^{18}O$-value of 2.5. Considering the mineral assemblage of the two rocks, in which ^{18}O-enriched minerals such as quartz are absent or minor, it seems likely that the $\delta^{18}O$ variation between the amphibolite and eclogite is the result of an external fluid/rock interaction during the retrogression of CCSD-3-Am. On the other hand, almost identical $\delta^{18}O$ values of both garnet and bulk rock between CCSD-4-Ec and CCSD-4-Am, and equilibrium oxygen isotope fractionation between garnet and amphibole in CCSD-4-Am (with mean $\delta^{18}O = 1.8$ and 2.1, respectively) indicate an internal fluid supply that caused the formation of the amphibolite, as internal fluids related to subduction processes usually do not change their $\delta^{18}O$ >0.2‰ compared with their precursor rocks (Cartwright and Barnicoat 1999).

Li and B behavior during retrograde metamorphism of UHP metamorphic rocks

Major and trace elements, oxygen, and Sr-Nd-Pb isotopic compositions indicate that sample sets 3 and 4 have formed in different environments, i.e., external and internal fluid/rock interaction systems, respectively. Therefore, Li and B isotopes provide an opportunity to investigate high-temperature Li and B isotopic fractionations under open- and closed-system conditions during exhumation of UHP metamorphic rocks.

Li and B isotopes are strongly fractionated between CCSD-3-Am and CCSD-3-Ec (open system), with

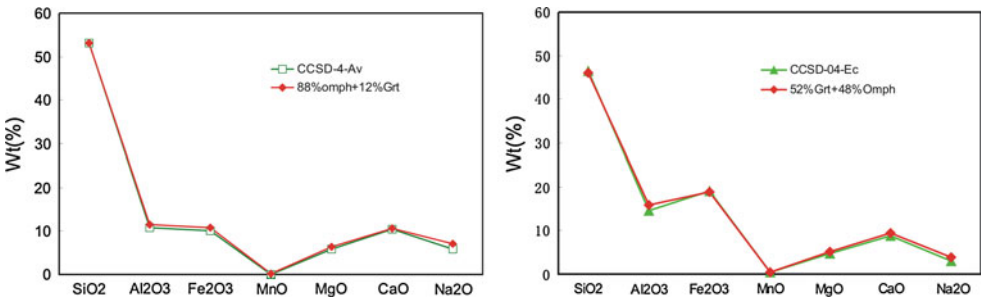

Fig. 8 Comparison between measured bulk major components and those calculated from microprobe data of omphacite and garnet in sample set 4. Modeling suggests that CCSD-4-Av composes of 88% omphacite + 12% garnet, whereas CCSD-4-Ec contains 48% omphacite and 52% garnet

δ^7Li = −6.5 and δ^{11}B = −9.3 in the eclogite, and significantly heavier values (+0.9 and −1.1, respectively) in the retrograded amphibolite, indicating an enrichment of ^{7}Li and ^{11}B in the amphibolite having reacted with an external fluid. Moreover, higher Li but lower B concentrations in the eclogite compared with the amphibolite (Table 4) indicate that, B has been added during fluid/rock interaction, whereas Li is more controlled by mineral characteristics rather than by the fluid alone, which is reflected by the much higher Cpx abundance in the eclogite than in the amphibolite.

In CCSD-4-Am and CCSD-4-Ec, representing an internally buffered fluid/rock system, the very similar B element concentration and isotopic compositions of eclogite and amphibolite indicate that B concentration and isotopic composition will not change significantly when the fluid is internally derived. On the other hand, Li concentration and isotopic composition are significantly different between eclogite and amphibolite (Table 4), suggesting significant Li elemental and isotopic fractionation under closed conditions. This again indicates that under high P–T conditions (amphibolite formation: temperatures are around 800°C), mineralogical differences rather than fluids will affect the Li budget and isotopic compositions of a rock.

Although at low temperatures (e.g., <300°C) both Li and B have similar small solid/fluid partition coefficients and the same isotopic fractionation trends, at higher temperatures, B behaves as a typical fluid-mobile element (Leeman and Sisson 1996), whereas Li concentration and isotopic composition are more reaction controlled than by fluid phases. During high-grade metamorphism (i.e., high T), Li and B thus may show different patterns of enrichment and of isotopic fractionation.

Conclusions

Four sample sets with contrasting lithological boundaries in UHP metamorphic rocks from the CCSD program provide information on element transfer and Li, B, and O as well as Sr-Nd-Pb isotopic features induced by fluid mobilization from subduction dehydration through peak metamorphism to exhumation rehydration processes in a continental subduction zone. During the various stages of UHP metamorphism, O and Sr-Nd-Pb isotopic compositions keep in general unchanged, but there is significant Li and/or B isotope fractionation between different rock types that are in close contact. An enrichment of Rb, Ba, Th, LREE, and other incompatible elements in a HP vein representing dehydration during prograde metamorphism is interpreted that vein formation is initiated by locally derived fluids that have leached elements from the dehydrated host rock. These fluids are water rich, with low contents of silicates at an early stage, but under UHP conditions become phases that are intermediate in composition between water and silicate melt. Partial melting is unlikely even under high water activity of vein-forming conditions, as partial melting will remove any phengite in the vein.

Due to lithological and structural heterogeneities of the subducting slab, the temporal and spatial distribution of fluids is heterogeneous within the slab. This is documented in a sample set consisting of garnet peridotite, a transition zone, and eclogite. The formation of chlorite and amphibole and compositionally different Cpx-II grains in the transition zone between eclogite and garnet peridotite clearly reveals the addition of hydrous fluids enriched in silicate component from the subducting slab to the mantle.

Investigations into retrogressive samples revealed that both external and internal fluids are plausible candidates that may have caused retrogression of UHP metamorphic rocks in the Dabie–Sulu area, depending on open or closed system conditions.

The overall large variations of δ^7Li from −6.9 to +2.5‰ and δ^{11}B from −9.3 to +11.7 in the investigated samples indicate significant Li and B isotopic fractionations during different metamorphic stages of the UHP rocks. Regardless of the origin of the δ^7Li and δ^{11}B variations observed in four sample sets, two important points should be emphasized. First, B and Li may behave differently during UHP metamorphism as their budget is probably controlled by fluid, melt, temperature, and mineral assemblages as well as diffusive processes, and most importantly by the previous history of fluid and mineral reactions. This is evident from the contrasting isotopic fractionation of Li and B in samples representing prograde metamorphism and those representing near-peak conditions and the contrasting correlation between element concentration and isotopic composition of the two elements. Second, Li and B isotopic compositions of retrograde amphibolite that may result from external fluid/rock interactions are consistent with experimental data on the fractionation behavior of Li and B among minerals and HP fluids. However, in a closed system (e.g., sample set 4), mineral assemblages seem controlling Li isotopic fractionations.

Acknowledgments Special thanks go to Dr. R. L Romer for his support in the analytical work. He introduced the first author to the radiogenic isotope (Sr, Nd, Pb) chemistry and performed the Sr-Nd-Pb isotope analysis. Mrs. A. Meixner was of great help for the Li and B isotope analysis and carried out the MC-ICPMS measurements. Analytical assistance from Mrs. C. Schulz is highly appreciated. Prof. ZQ Xu is thanked for her assistance during sample collection. Careful and constructive reviews by Horst Marschall and an anonymous reviewer and editorial comments by Tim Grove have substantially improved the manuscript. This study was financially supported by grants from the National Science Foundation of China (40773003, 40921002), the National Science Foundation of Germany (HO

375/22) the Academy of Science of China (kzcx2-yw-131), and the Major State Basic Research Development Program of China (2009 CB825002, 2003 CB716501).

References

Agostini S, Ryan JG, Tonarini S, Innocenti F (2008) Drying and dying of a subducted slab: coupled Li and B isotope variations in Western Anatolia Cenozoic Volcanism. Earth Planet Sci Lett 272:139–147

Aranovich LY, Pattison DRM (1995) Reassessment of the garnet-clinopyroxene Fe-Mg exchange thermometer. I. Evaluation of the Pattison and Newton (1989) experiments. Contrib Miner Petrol 119:16–29

Baker J, Matthews A, Mattey D, Rowley D, Xue F (1997) Fluid-rock interactions during ultra-high pressure metamorphism, Dabie Shan, China. Geochim Cosmochim Acta 61:1685–1696

Barnicoat AC, Fry N (1986) High-pressure metamorphism of the Zermatt-Saas ophiolite zone. J Geol Soc 143:607–618

Bebout GE (2007) Metamorphic chemical geodynamics of subduction zones. Earth Planet Sci Lett 260:373–393

Bebout GE, Barton MD (2002) Tectonic and metasomatic mixing in a high-T, subduction-zone melange—insights into the geochemical evolution of the slab-mantle interface. Chem Geol 187:79–106

Bebout GE, Ryan JG, Leeman WP (1993) B-Be systematics in subduction-realted metamorphic rocks: characterization of the subducted component. Geochim Cosmochim Acta 57:2227–2237

Becker H, Jochum K, Carlson R (1999) Constraints from high-pressure veins in eclogites on the composition of hydrous fluids in subduction zones. Chem Geol 160:291–308

Benton LD, Ryan GG, Tera F (2001) Boron isotope systematics of slab fluids as inferred from a serpentine seamount, Mariana forearc. Earth Planet Sci Lett 187:273–282

Benton LD, Ryan GG, Savov IP (2004) Lithium abundance and isotope systematics of forearc serpentinites Conical Seamount, Mariana forarc: insights into the mechanics of slab-mantle exchange during subduction. Geochem Geophy Geosyst 5. doi: 10.1029/2004GC000708

Carswell D, O'Brien P, Wilson R, Zhai M (1997) Thermobarometry of phengite-bearing eclogites in the Dabie Mountains of central China. J Metamorph Geol 2:239–252

Cartwright I, Barnicoat AC (1999) Stable isotope geochemistry of alpine ophiolites: a window to ocean floor hydrothermal alteration and constraints on fluid-rock interaction during high-pressure metamorphism. Int J Earth Sci 88:219–235

Castelli D, Rolfo F, Compagnoni R, Xu ST (1998) Metamorphic veins with kyanite, zoisite and quartz in the Zhu-Jia-Chong eclogite, Dabie Shan, China. Isl Arc 7:159–173

Chan LH, Edmond JM, Thompson G, Gillis K (1992) Lithium isotopic composition of submarine basalts: implications for the lithium cycle in the oceans. Earth Planet Sci Lett 108:151–160

Chazot G, Lowry D, Menzies M, Mattey D (1997) Oxygen isotopic composition of hydrous and anhydrous mantle peridotites. Geochim Cosmochim Acta 61:161–169

Chen RX, Zheng YF, Gong B, Zhao ZF, Gao TS, Chen B, Wu YB (2007) Origin of retrograde fluid in ultrahigh-pressure metamorphic rocks: constraints from mineral hydrogen isotope and water content changes in eclogite—gneiss transitions in the Sulu orogen. Geochim Cosmochim Acta 71:2299–2325

Dobrzhinetskaya L, Green HW, Wang S (1996) Alpe Arami: a peridotite massif from depths of more than 300 kilometers. Science 271:1841–1845

Domanik KJ, Hervig RL, Peacoak SM (1993) Beryllium and boron in subduction zone minerals- An ion microprobe study. Geochim Cosmochim Acta 57:4997–5010

Elliott T, Thomas A, Jeffcoate AB, Niu Y (2002) Li isotope variations in the upper mantle. Geochim Cosmochim Acta 66:A214

Elliott T, Jeffcoate A, Bouman C (2004) The terrestrial Li isotope cycle: light-weight constraints on mantle convection. Earth Planet Sci Lett 7032:1–15

Elliott T, Thomas A, Jeffcoate A, Niu Y (2006) Lithium isotope evidence for subduction-enriched mantle in the source of mid-ocean-ridge basalts. Nature 443:565–568

Ellis DJ, Green DH (1979) An experimental study of the effect of Ca upon garnet-clinopyroxene Fe-Mg exchange equilibriua. Contrib Miner Petrol 71:13–22

Forneris JF, Holloway JR (2003) Phase equilibria in subducting basaltic crust: implications for H2O release from the slab. Earth Planet Sci Lett 214:187–201

Franz L, Romer RL, Klemd R, Schmid R, Oberhansli R, Wagner T, Dong SW (2001) Eclogite-facies quartz veins within metabasites of the Dabie Shan (eastern China): pressure-temperature-time-deformation path, composition of the fluid phase and fluid flow during exhumation of high-pressure rocks. Contrib Miner Petrol 141:322–346

Gerya T, Stöckhert B (2006) Two-dimensional numerical modeling of tectonic and metamorphic histories at active continental margins. Int J Earth Sci 95:250–274

Gonfiantini R, Tonarini S, Groening M, Adorni-Braccesi A, Al-Ammar A, Astner M, Baehler S, Barnes R, Bassett R, Cocherie A, Deyhle A, Dini A, Ferrara G, Gaillardet J, Grimm J, Guerrot M, Kraehenbuehl U, Layne G, Lemarchand D, Meixner A, Northington D, Pennisi M, Reitznerova E, Rodushkin I, Sugiura N, Surberg R, Tonn S, Wiedenbeck M, Wunderli S, Xiao Y, Zack T (2003) Intercomparison of boron isotope and concentration measurements. Part II: evaluation and results. Geostand Newsl J Geostand Geoanal 27:41–57

Green DH, Ringwood AE (1967) The stability fields of alumunous pyroxene peridotite and garnet peridotite and their relevance in upper mantle structure. Earth Planet Sci Lett 3:151–160

Harley SL (1984) The solubility of alumina in orthopyroxene coexisting with garnet in Feo-MgO-Al_2O_3-SiO_2. J Petrol 25:665–696

Harley SL, Green DH (1982) Garnet orthopyroxene barometry for granulites and peridotites. Nature 300:697–701

Hervig RL, Moore GM, Williams LB, Peacock SM, Holloway JR, Roggansack K (2002) Isotopic and elemental partitioning of boron between hydrous fluid and silicate melt. Am Miner 87:769–774

Hoefs J, Sywall M (1997) Lithium isotope composition of Quaterary and Tertiary biogen carbonates and global lithium isotope balance. Geochim Cosmochim Acta 61:2679–2690

Ionov DA, Seitz H (2009) Lithium abundances and isotopic compositions in mantle xenoliths from subduction and intra-plate settings: mantle sources vs. eruption histories. Earth Planet Sci Lett 266:316–331

Ishikawa T, Nakamura E (1994) Origin of the slab component in arc lavas from across-arc variation of B and Pb isotopes. Nature 370:205–208

James RH, Allen DE, Seyfried WE (2003) An experimental study of alteration of oceanic crust and terrigenous sediments at moderate temperatures (51 to 350 C8): insights as to chemical processes in near-shore ridge-flank hydrothermal systems. Geochim Cosmochim Acta

Jarrard RD (2003) Subduction fluxes of water, carbon dioxide, chlorine, and potassium. Geochem Geophys Geosyst 4:8905

Jeffcoate AB, Elliott T, Thomas A, Bouman C (2004) Precise, small sample size determinations of Lithium isotopic compositions of

geological reference materials and modern seawater by MC-ICP-MS. Geostand Newslett J Geostand Geoanal 28:161–172
John BM (1998) Geochemical and isotope characteristics of UHP eclogites and ultramafic rocks of the Dabie Orogen: implications for continental subduction and collisional tectonics. In: Hacker BR, Liou JG (eds) When Continents Collide: Geodynamics and Geochemistry of Ultrahigh-pressure Rocks. Kluwer, Dordrecht, pp 203–239
Kasemann S, Meixner A, Rocholl A, Vennemann T, Rosner M, Schmitt A, Wiedenbeck M (2001) Boron and oxygen isotope composition of certified reference materials NIST SRM 610/612 and reference material JB-2 and JR-2. Geostand Newslett J Geostand Geoanal 25:405–416
Kessel R, Schmidt MW, Ulmer P, Pettke T (2005) Trace element signature of subduction-zone fluids, melts and supercritical liquids at 120–180 km depth. Nature 437:724–727
King RL, Kohn MJ, Eiler JM (2003) Constraints on the petrologic structure of the subduction zone slab-mantle interface from Franciscan Complex exotic ultramafic blocks. Geol Soc Am Bull 115:1097–1109
Kisakurek B, Widdowson M, James RH (2004) Behaviour of Li isotopes during continental weathering: the Bidar laterite profile, India. Chem Geol 72:27–44
Kohler J, Schonenberger J, Upton B, Markl G (2009) Halogen and trace-element chemistry in the Gardar Province, South Greenland: subduction-related mantle metasomatism and fluid exsolution from alkalic melts. Lithos 113:731–747
Krogh EJ (1988) The garnet-clinopyroxene Fe-Mg geothermometer—a reinterpretation of existing experimental data. Contrib Miner Petrol 99:44–48
Lee HY, Ganguly J (1988) Equilibrium compositions of coexisting garnet and orthopyroxene: experimental determinations in the system FeO-MgO-Al_2O_3-SiO_2, and applications. J Petrol 29:93–113
Lee CT, Oka M, Luffi P, Agranier A (2008) Internal distribution of Li and B in serpentinites from the Feather River Ophiolite, California, based on laser ablation inductively coupled plasma mass spectrometry. Geochem Geophys Geosyst Q12011. doi: 10.1029/2008GC002078
Leeman WP, Sisson VB (1996) Geochemistry of boron and its implications for crustal and mantle processes. Rev Miner 33:645–707
Leeman WP, Tonarini S, Chan LH, Borg LE (2004) Boron and lithium isotopicvariations in a hot subduction zone—the southern Washington Cascades. Chem Geol 212:101–124
Li SG, Xiao YL, Liu DL, Chen YZ, Ge NG, Zhang ZQ, Sun SS, Cong BL, Zhang RL, Hart SR, Wang SS (1993) Collision of the North China and Yangtse Blocks and formation of coesite-bearing eclogites: timing and processes. Chem Geol 109:89–111
Li SG, Jagoutz E, Chen YZ, Li QL (2000) Sm-Nd and Rb-Sr isotopic chronology and cooling history of ultrahigh pressure metamorphic rocks and their country rocks at Shuanghe in the Dabie Mountains, Central China. Geochim Cosmochim Acta 64:1077–1093
Li SG, Huang F, Zhou H, Li H (2003) U-Pb isotopic compositions of the ultrahigh pressure metamorphic (UHPM) rocks from Shuanghe and gneisses from Northern Dabie zone in the Dabie Mountains, central China: constraint on the exhumation mechanism of UHPM rocks. Sci China (D) 46:200–209
Li XP, Zheng YF, Wu YB, Chen FK, Gong B, Li YL (2004) Low-T eclogite in the Dabie terrane of China: petrological and isotopic constraints on fluid activity and radiometric dating. Contrib Miner Petrol 148:443–470
Li SG, Wang CX, Dong F, Hou ZH, Li QL, Liu YC, Huang F, Chen FK (2009) Common Pb of UHP metamorphic rocks from the CCSD project (100–5000 m) suggesting decoupling between the slices within subducting continental crust and multiple thin slab exhumation. Tectonophysics 475:308–317
Liu FL, Xu ZQ, Liou JG, Dong HL, Xue HM (2007) Ultrahigh-Pressure mineral assemblages in zircons from the surface to 5158 m depth in cores of the main drill hole, Chinese Continental Scientific Drilling Project, Southwestern Sulu Belt. China Int Geol Rev 49:454–478
Magna T, Wiechert U, Grove TL, Halliday AN (2006) Lithium isotope fractionation in the southern Cascadia subduction zone. Earth Planet Sci Lett 250:428–443
Malaspina N, Poli S, Fumagalli P (2009) The oxidation state of metasomatized mantle wedge: insights from C-O-H-bearing garnet peridotite. J Petrol 50:1533–1552
Marocchi M, Hermann J, Morten L (2007) Evidence for multi-stage metasomatism of chlorite-amphibole peridotites (Ulten Zone, Italy): constraints from trace element compositions of hydrous phases. Lithos 99:85–104
Marocchi M, Mair V, Tropper P, Bargossi G (2009) Metasomatic reaction bands at the Mt. Hochwart gneiss-peridotite contact (Ulten Zone, Italy): insights into fluid-rock interaction in subduction zones. Miner Petrol 95:251–272
Marschall H, Altherr R, Ludwig T, Kalt A, Gmeling K, Kasztovszky Z (2006) Partitioning and budget of Li, be and B in high-pressure metamorphic rocks. Geochim Cosmochim Acta 70:4750–4769
Marschall H, von Strandmann P, Seitz H, Elliott T, Niu Y (2007a) The lithium isotopic composition of orogenic eclogites and deep subducted slabs. Earth Planet Sci Lett 262:563–580
Marschall H, Altherr R, Rüpke L (2007b) Squeezing out the slab-modelling the release of Li, Be and B during progressive high-pressure metamorphism. Chem Geol 239:323–335
Massone HJ, Schreyer W (1987) Phengite geobarometry based on the limiting assemblage with K-feldspar, phlogopite, and quartz. Contrib Miner Petrol 96:212–224
Meyer C, Wunder B, Meixner A, Romer RL, Heinrich W (2008) Boron-isotope fractionation between tourmaline and fluid: an experimental re-investigation. Contrib Miner Petrol 156:259–267
Moriguti T, Nakamura E (1998) Across-arc variation of Li isotopes in lavas and implications for crust/mantle recycling at subduction zones. Earth Planet Sci Lett 163:167–174
Moriguti T, Shibata T, Nakamura E (2004) Lithium, boron and lead isotope and trace element systematics of Quaternary basaltic volcanic rocks in northeastern Japan: mineralogical controls on slab-derived fluid composition. Chem Geol 212:81–100
Morris JD, Leeman WP, Tera F (1990) The subducted component in island arc lavas: constraints from beryllium isotopes and B systematics. Nature 344:31–36
Nakano T, Nakamura E (1998) Static multicollection of Cs2BO2 + ions for precise boron isotope analysis with positive thermal ionization mass spectrometry. Int J Mass Spectrom 176:13–21
Niu YL (2004) Bulk-rock major and trace element compositions of abyssal peridotites: implications for mantle melting, melt extraction and post-melting processes beneath mid-ocean ridges. J Petrol 45:2423–2458
O'Neill HSC (1981) The transition between spinel lherzolite and garnet lherzolite, and its use as a Geobarometer. Contrib Miner Petrol 77:185–194
Ottolini L, Le Fevre B, Vannucci R (2004) Direct assessment of mantle boron and lithium contents and distribution by SIMS analyses of peridotite minerals. Earth Planet Sci Lett 228:19–36
Palmer MR, Swihart GH (1996) Boron isotope geochemistry: an overview. Rev Miner 33:709–744
Paquin J, Altherr R (2002) Subduction-related lithium metasomatism during exhumation of the Alpe Arami ultrahigh-pressure garnet peridotite (Central Alps, Switzerland). Contrib Miner Petrol 143:623–640

Paquin J, Altherr R, Ludwig T (2004) Li-Be-B systematics in the ultrahigh-pressure garnet peridotite from Alpe Arami (Central Swiss Alps): implications for slab-to-mantle wedge transfer. Earth Planet Sci Lett 218:507–519

Peacock SM (1990) Fluid processes in subduction zones. Science 248:329–337

Poli S, Schmidt MW (1995) H2O transport and release in subduction zones: experimental constrains on basaltic and andesitic systems. J Geophys Res 100:22299–22314

Rapp RP, Watson EB (1995) Dehydration melting of metabasalt at 8–32-kbar—implications for continental growth and crust-mantle recycling. J Petrol 36:891–931

Ravna EK (2000) Distribution of Fe^{2+} and Mg between coexisting garnet and hornblende in synthetic and natural systems: an empirical calibration of the garnet-hornblende Fe-Mg geothermometer. Lithos 53:265–277

Robinson CJ, Wood BJ (1998) The depth of the spinel to garnet transition at the peridotite solidus. Earth Planet Sci Lett 164:277–284

Romer RL, Heinrich W, Schroer-Smeibidl B, Meixner A, Fischer CO, Schulz C (2005) Elemental dispersion and stable isotope fractionation during reactive fluid-flow and fluid immiscibility in the Bufa del Diente aureole, NE-Mexico: evidence from radiographies and Li, B, Sr, Nd, and Pb isotope systematics. Contributions Miner Petrol 149:400–429

Rudnick RL, Tomascak PB, Njo HB, Gardner LR (2004) Extreme lithium isotopic fractionation during continental weathering revealed in sapprolites from South Carolina. Chem Geol 72:45–47

Salters VJM, Stracke A (2004) Composition of the depleted mantle. Geochem Geophy Geosyst 5:1–27

Schmidt MW, Dardon A, Chazot G, Vannucci R (2004a) The dependence of Nb and Ta rutile-melt partitioning on melt composition and Nb/Ta fractionation during subduction processes. Earth Planet Sci Lett 226:415–432

Schmidt MW, Vielzeuf D, Auzanneau E (2004b) Melting and dissolution of subducting crust at high pressures: the key role of white mica. Earth Planet Sci Lett 228:65–84

Seitz H-J, Brey GP, Lahaye Y, Durali S, Weyer S (2004) Lithium isotopic signatures of peridotite xenoliths and isotopic fractionation at high temperatures between olivine and pyroxenes. Chem Geol 212:163–177

Seyfried WE, Chen X, Chan LH (1998) Trace element mobility and lithium isotope exchange during hydrothermal alteration of seafloor weathered basalt: an experimental study at 350 degrees C, 500 bars. Geochim Cosmochim Acta 62:949–960

Simons KK, Harlow GE, Brueckner HK, Goldstein SL, Sorensen SS, Hemming NG, Langmuir CH (2010) Lithium isotopes in Guatemalan and Franciscan HP-LT rocks: insights into the role of sediment-derived fluids during subduction. Geochim Cosmochim Acta 74:3621–3641

Spandler C, Hermann J (2006) High-pressure veins in eclogite from New Caledonia and their significance for fluid migration in subduction zones. Lithos 89:135–153

Su W, Ji ZP, Ye K, You ZD, Liu JB, Yu J, Cong BL (2004) Distribution of hydrous components in jadeite of the Dabie Mountains. Earth Planet Sci Lett 222:85–100

Sun SS, McDonough WF (1989) Chemical and isotopic systematics of oceanic basalts: implication for mantle composition and processes. In: Saunders AD, Norry MJ (eds) Magamtism in the Ocean Basins. Geological Society of London Special Publication, vol 42, pp 313–345

Teng F, McDonough W, RL R, Wing B (2007) Limited lithium isotopic fractionation during progressive metamorphic dehydration in metapelites: a case study from the Onawa contact aureole, Maine. Chem Geol 239:1–12

Thompson AB (1992) Water in the Earth's upper mantle. Nature 358:295–302

Tomascak PB (2004) Developments in the understanding and application of lithium isotopes in the Earth and planetary sciences. Rev Miner 55:153–195

Tomascak PB, Tera F, Helz RT, Walker RJ (1999) The absence of lithium isotope fractionation during basalt differentiation: new measurements by multicollector sector ICP-MS. Geochim Cosmochim Acta 63:907–910

Tomascak PB, Widom E, Benton LD, Goldstein SL, Ryan JG (2002) The control of lithium budgets in island arcs. Earth Planet Sci Lett 196:227–238

Tonarini S, Pennisi M, Leeman WP (1997) Precise boron isotopic analysis of complex silicate (rock) samples using alkali carbonate fusion and ion-exchange separation. Chem Geol 142:129–137

Vils F, Pelletier L, Kalt A, Müntener O, Ludwig T (2008) The Lithium, Boron and Beryllium content of serpentinized peridotites from ODP Leg 209 (Sites 1272A and 1274A): implications for lithium and boron budgets of oceanic lithosphere. Geochim Cosmochim Acta 72:5475–5504

Wawrzenitz N, Romer RL, Oberhaesli R, Dong SW (2006) Dating of subduction and differential exhumation of UHP rocks from the Dabie Complex (E-China): constraints from microfabrics, Rb-Sr and U-Pb isotope systems. Lithos 89:174–201

Wiechert U, Fiebig J, Przybilla R, Xiao Y, Hoefs J (2002) Excimer laser isotope-ratio-monitoring mass spectrometry for in situ oxygen isotope analysis. Chem Geol 182:179–194

Woodland AB, Seitz HM, Altherr R, Marschall H, Olker B, Ludwig T (2002) Li abundances in eclogite minerals: a clue to a crustal or mantle origin? Contrib Miner Petrol 143:587

Wu YB, Gao S, Zhang HF, Yang SH, Liu XC, Jiao WF, Liu YS, Yuan HL, Gong HJ, He MC (2009) U-Pb age, trace-element, and Hf-isotope compositions of zircon in a quartz vein from eclogite in the western Dabie Mountains: constraints on fluid flow during early exhumation of ultra high-pressure rocks. Am Miner 94:303–312

Wunder B, Meixner A, Romer RL, Wirth R, Heinrich W (2005) The geochemical cycle of boron: constraints from boron isotope partitioning experiments between mica and fluid. Lithos 84:206–216

Wunder B, Meixner A, Romer RL, Heinrich W (2006) Temperature-dependent isotopic fractionation of lithium between clinopyroxene and high-pressure hydrous fluids. Contrib Miner Petrol 151:112–120

Xia QK, Sheng YM, Yang XZ, Yu HM (2005) Heterogeneity of water in garnets from UHP eclogites, eastern Dabieshan, China. Chem Geol 224:237–246

Xiao YL, Hoefs J, van den Kerkhof AM, Fiebig J, Zheng YF (2000) Fluid history of UHP metamorphism in the Dabie Shan, China: a fluid inclusion and oxygen isotope study on the coesite-bearing eclogite from Bixiling. Contrib Miner Petrol 139:1–16

Xiao YL, Zhang ZM, Hoefs J, van den Kerkhof A (2006) Ultrahigh-pressure metamorphic rocks from the Chinese Continental Scientific Drilling Project: II. Oxygen isotope and fluid inclusion distributions through vertical sections. Contrib Miner Petrol 152:443–458

Xu ZQ (2007) Continental deep subduction and exhumation dynamics: evidence from the main hole of the Chinese Continental Scientific Drilling and the Sulu HP-UHP metamorphic terrane. Acta Petrol Sinica 23:3041–3053

Yang JS, Li TF, Liang FH, Wu CL, Chen SY (2007) Garnet peridotite in CCSD-MH in the Sulu UHPM belt: a deep subducted Plaeozoic ultramafic intrusion. Acta Petrol Sinica 23:3153–3170

You C, Spivack A, Smith J, Gieskes J (1993) Mobilization of boron in convergent margins—implications for the boron geochemical cycle. Geology 21:207–210

Yui TF, Rumble D, Chen CH, Lo CH (1997) Stable isotope characteristics of eclogites from the ultra-high-pressure metamorphic terrain, east-central China. Chem Geol 137:135–147

Zack T, Foley SF, Rivers T (2002) Equilibrium and disequilibrium trace element partitioning in hydrous eclogites (Trescolmen, Central Alps). J Petrol 43:1947–1974

Zack T, Tomascak PB, Rudnick RL, Dalpe C, McDonough WF (2003) Extremely light Li in orogenic eclogites: the role of isotopic fractionation during dehydration in subducted oceanic crust. Earth Planet Sci Lett 208:279–290

Zhang ZM, Xiao YL, Hoefs J, Liou JG, Simon K (2006) UHP metamorphic rocks from the Chinese continental scientific drilling project: I. Petrology and geochemistry of the main hole (0–2050 m). Contrib Miner Petrol 152:421–441

Zhang RY, Li TF, Rumble D, Yui TF, Li L, Yang JS, Pan Y, Liou JG (2007) Multiple metasomatism in Sulu ultrahigh-P garnet peridotite constrained by petrological and geochemical investigations. J Metamorph Geol 25:149–164

Zhang ZM, Shen K, Sun WD, Liu YS, Liou JG (2008) Fluids in deeply subducted continental crust: petrology, mineral chemistry and fluid inclusion of UHP metamorphic veins from the Sulu orogen, eastern China. Geochim Cosmochim Acta 72:3200–3228

Zhang RY, Liou JG, Ernst WG (2009a) The Dabie-Sulu continental collision zone: a comprehensive review. Gondwana Res 16:1–26

Zhang ZM, Schertl HP, Wang JL, Shen K, Liou JG (2009b) Source of coesite inclusions within inherited magmatic zircon from Sulu UHP rocks, eastern China, and their bearing for fluid-rock interaction and SHRIMP dating. J Metamorph Geol 27:317–333

Zhao ZF, Zheng YF, Wei CS, Wu YB (2007) Post-collisional granitoids from the Dabie orogen in China: Zircon U-Pb age, element and O isotope evidence for recycling of subducted continental crust. Lithos 93:248–272

Zheng YF (1993) Calculation of oxygen isotope fractionation in hydroxyl-bearing silicates. Earth Planet Sci Lett 120:247–263

Zheng YF (2009) Fluid regime in continental subduction zones: petrological insights from ultrahigh-pressure metamorphic rocks. J Geol Soc 166:763–782

Zheng YF, Gao TS, Wu YB, Gong B, Liu XM (2007) Fluid flow during exhumation of deeply subducted continental crust: zircon U-Pb age and O-isotope studies of a quartz vein within ultrahigh-pressure eclogite. J Metamorph Geol 25:267–283